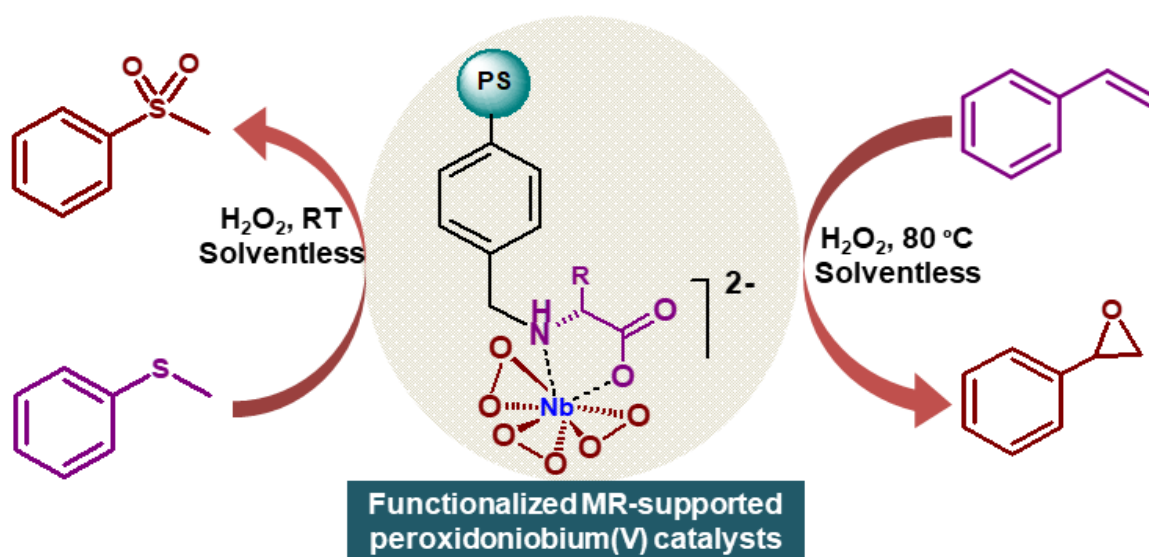# CHAPTER 3

Niobium(V)-Peroxido Complexes Supported on Organic Polymer as Sustainable Catalysts for Solventless Olefin Epoxidation and Sulfide Oxidation

Functionalized MR-supported peroxidoniobium(V) catalysts

3.1 Introduction

The mounting environmental concerns in recent times have triggered a dramatic upsurge in interest in the development of safer and sustainable alternative synthetic routes to target compounds [1-4]. Among the vast range of organic oxidations, epoxidation of olefins, as well as oxidation of organosulfur compounds to sulfoxide or sulfone, are outstanding industrial transformations representing the basis of a variety of chemical processes for the production of commodity and fine chemicals [5-11]. Moreover, the sulfide-oxidation based procedure of oxidative desulfurization has been recognized as a greener alternative method for the removal of sulfur from fuel feedstock [12,13].

The use of heterogeneous catalysts that support clean and energy-efficient transformations and can perform optimally in absence of hazardous organic solvents, are emerging as issues of paramount importance in green synthetic strategy [1,3,4]. Organic-solvent-free synthesis in addition to being cost-effective, contributes significantly towards waste minimization and environmental protection and thus displays tremendous application potential for larger-scale chemical processes [14-20]. Lately, a considerable number of innovative and active heterogeneous catalysts, mostly based on metals such as Mn, Ni, Ti, V, Mo and W, have been reported, especially for the solvent-less epoxidation of olefins [15-24]. However, majority of the reported non-solvent processes utilized toxic and volatile organic hydroperoxides like cumene hydroperoxide (CHP) and *tert*-butyl hydroperoxide (TBHP) as oxidizing agents under anhydrous condition and required elevated temperature for attaining high activity [16-21,23,24]. These factors significantly compromise the sustainability standard of such otherwise effective procedures.

It is intriguing to note that, niobium-based solid catalysts so far have rarely been tested in solvent-free organic oxidations, although such systems were often reported to display superior activity when aqueous hydrogen peroxide was used as a terminal oxidant [7,25-27]. This feature offers a significant advantage as catalytic epoxidation of olefins with aqueous H_2O_2, is the focus of much contemporary research [3,4]. Aqueous H_2O_2, with its high oxygen content, has been recognized as the greener and more desirable choice among the variety of available terminal oxidants as it's economical, non-polluting and safe [1-4]. As has already been highlighted in the introductory Chapter, work from several laboratories has demonstrated that silica supported Nb(V) catalysts are highly stable towards hydrolysis and metal leaching, and such systems were observed to provide faster oxidation rates compared to the more standard Ti-SiO$_2$ catalysts [25,28-32]. Nevertheless,

most of the existing Nb-based heterogeneous catalysts, including the ones supported on mesoporous materials, as revealed by survey of literature, often provided low to moderate conversion and turnover number (TON) in H_2O_2 induced alkene epoxidations conducted in presence of various organic solvents [7,25,30,33-38]. In fact, porous siliceous oxide or other metal oxide-based supports have often been linked to a number of drawbacks with respect to catalytic activity and selectivity [39,40]. In this context, it is somewhat surprising that no attempts appear to have been made till date to develop Nb-based solid catalysts for organic oxidations, using organic polymers as support. The practical utility of organic polymers, which are known to be generally non-toxic, non-volatile and inert [41-46], for heterogenization of homogeneous catalysts have been adequately emphasized in the literature [41-47] as well as in Chapter 1. Being insoluble and recyclable, the polymer supported systems usually offers the benefits of both homogeneous and heterogeneous catalysts by reducing the limitations associated with both types of systems [41-47].

Motivated by the aforementioned observations, in the present study, our objective has been to explore the possibility of generating new heterogeneous catalyst system for organic oxidations, by incorporating active peroxidoniobium species into appropriately functionalized Merrifield resin (**MR**). As has been described in Chapter 1, **MR** or poly(styrene-divinylbenzene) resin (PS-DVB) still stands out as one of the most versatile macromolecular supports for catalytic applications. It has been observed that **MR** functionalized with simple and easily available bifunctional ligand (N,O-donor) such as amino acid, served as effective support for facile coordination of peroxidometal species leading to robust metal-polymer linkage [48,49]. Moreover, such multidentate ligands offered the prospect of obtaining site isolated stable peroxidoniobium grafted stable catalysts. Recently, single-site heterogeneous niobium catalysts or supported catalysts that ensure Nb atom site isolation during catalytic turnover has been receiving great deal of importance [50,51]. Such systems are known to provide good stability along with high activity and selectivity under turnover conditions of liquid phase oxidations with H_2O_2 [50,51].

Here we present the preparation of a set of heretofore unreported polymer anchored peroxidoniobium complexes which are employed for the epoxidation of a variety of olefins, as well as selective oxidation of sulfides to sulfone, under solvent-free mild conditions. The efficiency of the developed catalytic protocols is discussed in terms of

their TON, H_2O_2 efficiency, reusability, and eco-compatibility. Interestingly, except for one report on cyclooctene epoxidation catalyzed by Nb-MCM-41 catalysts [24], we are yet to come across work on alkene epoxidation or sulfide oxidation using solid Nb-based catalysts under solventless condition.

3.2 Experimental section

3.2.1 Functionalization of the polymer support with amino acids

The anchoring of amino acids (**AA**) L-valine (**MRV**), L-asparagine (**MRN**) or glycine (**MRG**) to the polymer resin was accomplished by a procedure described earlier in detail [48-49,52]. Briefly, 2 g (5 mmol of Cl⁻) of pre-washed PS-DVB beads were swelled in methanol (6 mL) for 1 h. An aqueous solution containing 6.25 mmol of the amino acid, L-valine (0.73 g), L-asparagine (0.83 g) or glycine (0.47 g) prepared in 20 mL of water was added to that swollen polymer in methanol. After refluxing for 24 h at 90 °C in presence of pyridine (0.50 mL, 6.25 mmol) maintaining the overall molar ratio of Cl⁻**:** amino acid**:** pyridine on the basis of percent replaceable chlorine on polymer at approximately 1**:**1.25**:**1.25, the resulting mixture was cooled and kept for one week at room temperature with occasional stirring. The distinct colour change of the polymer beads from pale white to yellow showed the incorporation of the amino acid into the polymer. The amino acid-linked polymer beads were then filtered off and washed repeatedly using hot water until the precipitation of AgCl was stopped while the filtrate was treated with $AgNO_3$. The washing process was continued with ethanol and the obtained beads of **MRV**, **MRN**, or **MRG** were vacuum dried for 8 h at 90 °C.

3.2.2 Preparation of sodium tetraperoxidoniobate (TpNb) [53]

$Na_3[Nb(O_2)_4]\cdot13H_2O$, was synthesized using the reported method [53]. Nb_2O_5 (1 g) and NaOH (1.85 g) were fused together in a nickel crucible at 700 °C. The resulting solid product was cooled and dissolved in 100 ml of 1 M aqueous hydrogen peroxide by continuously stirring. After filtering the solution, the filtrate was kept for 24 h at 5 °C to obtain $Na_3[Nb(O_2)_4]\cdot13H_2O$ as a white crystalline product.

3.2.3 Synthesis of polymer immobilized triperoxidoniobium compounds (3.1-3.3)

In a typical reaction**,** the precursor complex sodium tetraperoxidoniobate ($Na_3[Nb(O_2)_4]\cdot13H_2O$) (1.25 mmol) was dissolved in 30% H_2O_2 (4 mL, 35.39 mmol). The

pH of the solution was observed to be *ca*. 6. Keeping the solution at ice bath condition i.e., below 4 °C, 1 g of **MRV**, **MRN**, or **MRG** (pre-swelled in 5 mL ethanol) was added to it and constantly stirred for 24 hours. After removing the supernatant liquid by decantation, the resulting yellowish residue was continuously washed with acetone, and finally the product, $[Nb(O_2)_3L]^{2-}$–**MR**, [L = valine (**MRVNb**) (**3.1**), asparagine (**MRNNb**) (**3.2**) or glycine (**MRGNb**) (**3.3**)] was separated by centrifugation and dried *in vacuo* over concentrated sulfuric acid.

3.2.4 General procedure for catalytic epoxidation of olefins

In a representative procedure, to a stirred reaction mixture consisting of catalyst (containing 0.005 mmol of Nb) [**MRVNb** (16.7 mg), **MRNNb** (13.9 mg), or **MRGNb** (18.5 mg)] and styrene (5 mmol), in a round-bottomed flask, 30% H_2O_2 (1.13 mL, 10 mmol) was added to initiate the chemical process. The reaction was conducted at 80 °C, maintaining the molar ratio of Nb: styrene: oxidant at 1:1000:2000. The reaction mixture turned cloudy at 80 °C due to the partially miscible organic substrate with aqueous H_2O_2 and the distinct phase separation between the aqueous and organic phases nearly disappeared. Aliquots of the reaction mixture were taken out periodically after stopping the stirring to settle down the solid catalyst and introduced to HPLC (high performance liquid chromatography) for progress monitoring and analysis (**Appendix I**). The samples were extracted with ethyl acetate. The catalyst was separated from the completed reaction mixture by filtration and washed with acetone for further use.

A Thermo-Scientific Dionex Ultimate 3000 HPLC system equipped with a UV detector was used for the quantitative analysis of styrene and its oxidized products. The system was set at 254 nm detection wavelength, and the products were well separated by the reversed-phase C18 column (250 × 4.6 mm). A mixture of acetonitrile, water, and methanol at a volume ratio of 2:5:3 was used as the mobile phase with an injection volume of 20 μL and a flow rate of 1 mL/min. Authentic samples of the substrate and products were used for identification. The content of the reaction mixtures was determined by the direct interpolation of the calibration curve which was generated by using the authentic samples of styrene and the oxidized products with 20-100 ppm of concentration range. The conversion of styrene (ST) and the selectivity of styrene oxide (STO) and benzaldehyde (BA) were calculated by using the following equations:

$$\text{Conversion of styrene } (X_{ST}) = \frac{[ST]_i - [ST]_f}{[ST]_i} \times 100\% \quad (3.1)$$

$$\text{Selectivity of STO } (S_{STO}) = \frac{[STO]}{[STO] + [BA]} \times 100\% \quad (3.2)$$

$$\text{Selectivity of BA } (S_{BA}) = \frac{[BA]}{[STO] + [BA]} \times 100\% \quad (3.3)$$

where [ST], [STO] and [BA] represent concentration of styrene, styrene oxide and benzaldehyde, respectively. i and f signify initial and final, respectively.

TON and TOF were calculated from the following equations:

$$\text{Turnover number (TON)} = \frac{\text{mmol of substrate consumed}}{\text{mmol of Nb}} \quad (3.4)$$

$$\text{Turnover frequency (TOF)} = \frac{\text{mmol of substrate consumed}}{\text{mmol of Nb} \times \text{Time}} \quad (3.5)$$

3.2.5 General procedure for oxidation of sulfides

The catalytic protocol for the oxidation of sulfides was as follows: catalyst (0.005 mmol of Nb) [**MRVNb** (16.7 mg), **MRNNb** (13.9 mg), or **MRGNb** (18.5 mg)] and 5 mmol of the substrate was placed in a 50 mL two-necked round-bottomed flask. With constant magnetic stirring at room temperature, 50% H_2O_2 (0.68 mL, 10 mmol) was added to the reaction mixture. The molar ratio of Nb: MPS: oxidant was fixed at 1:1000:2000. Thin-layer chromatography (TLC) and GC were used to monitor the progress of the reaction. As the reaction was completed, the catalyst was separated from the mixture by filtering and repeatedly washed with acetone. The unreacted organic substrates, also the products of the reaction were extracted using diethyl ether and dried with anhydrous Na_2SO_4 subsequently distilled under reduced pressure to remove the excess of diethyl ether. Column chromatography was carried out to purify the products where ethyl acetate: hexane (1:9) was used as the mobile phase. IR, NMR spectral analysis, and melting point determination were mainly applied for the characterization of the obtained products (**Appendix II**).

3.2.6 Procedure for control experiments

The control experiment for olefin epoxidation was conducted in the absence of the catalyst at 80 °C using styrene (5 mmol) as the model substrate under solvent-free

condition. The reaction was initiated by the addition of 30% H_2O_2 (1.13 mL, 10 mmol), and the progress of the reaction was monitored over a span of 6 h. For sulfide oxidation, the blank reaction was carried out with 5 mmol of the MPS and 10 mmol of 50% H_2O_2 maintaining a molar ratio of MPS: oxidant at 1:2 without the addition of the catalyst and solvent at room temperature.

3.2.7 Regeneration of the catalyst

For epoxidation, the recyclability of the catalysts was studied by carrying out the reaction with styrene. As mentioned earlier, after completion of the reaction, the solid catalyst was recovered by filtration, washed with acetone, and then dried *in vacuo*. The next cycle proceeded with the recovered catalyst and a fresh reaction mixture of styrene and 30% H_2O_2 under the optimized condition. HPLC was used to monitor the reaction progress.

In the case of oxidation of MPS to sulfone, the solid catalyst separated after the completion of the reaction was used with a fresh batch of reaction mixture containing 5 mmol of MPS and 10 mmol of 50% H_2O_2 to carry forward the next cycle under the standardized condition. In each case, up to five reaction cycles, the oxidation reactions were repeated. EDX Anal. found (regenerated catalyst **MRVNb** (**3.1**) after 5th cycle): C, 58.94; N, 2.79; Na, 7.62; Nb, 2.73%.

3.3   Results and discussion

3.3.1 Synthesis

The immobilized peroxidoniobium complexes **3.1-3.3** were prepared by adopting a two-step synthetic strategy. The step-wise modification of the PS-DVB resin, as shown in **Scheme 3.1**, involved functionalization of the polymer with the desired amino acid ligand, followed by the attachment of the Nb complexes by direct reaction of the derivatized polymer with the precursor complex, $Na_3[Nb(O_2)_4]$ in presence of hydrogen peroxide. Maintenance of near-neutral pH of *ca*. 6, the temperature at <4 ℃, and contact time of 24 h were found to be important factors in order to obtain the desired solid compounds. The composition of peroxidoniobium species in aqueous solution has been observed to be influenced by various factors including pH, Nb and peroxide concentration, as well as reaction temperature [54]. Co-workers of our group have also found previously that triperoxido-Nb species could be effectively stabilized *via* carboxylate coordination

maintaining pH of *ca*. 6 at <4 °C temperature [55]. It is notable that, the complexes were found to remain stable and active for weeks.
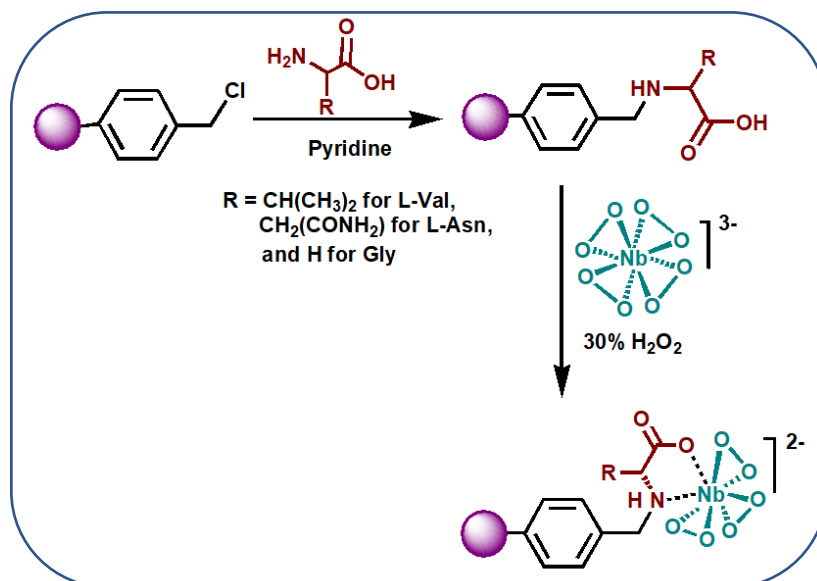
Scheme 3.1 Synthesis of PS-DVB-supported pNb complexes. "⬤" represents polymer chain.

3.3.2 Characterization

The complexes were characterized by a combination of analytical and spectroscopic techniques *viz*. FT-IR, Raman, ^{13}C NMR, powder XRD, ICP-OES, SEM-EDX, XPS, BET, and TG-DTG analysis. The analytical data presented in **Table 3.1** revealed that, asparagine grafted resin (**MRN**) was formed by replacement of nearly 88% of Cl$^-$ of -CH$_2$Cl groups of **MR**, whereas in the case of **MRV** and **MRG** *ca*. 82 and 77% of Cl$^-$ were replaced by valine and glycine, respectively. A ratio of 1:3 was obtained for Nb: peroxide from the elemental analysis data, which indicated the presence of three peroxido groups per niobium center in each of the compounds. The niobium loading on the compounds **MRVNb (3.1), MRNNb (3.2)** and **MRGNb (3.3)** corresponds to 0.30, 0.36 and 0.27 mmol per gram of the polymer, respectively. The complexes were observed to be diamagnetic in nature in accord with the occurrence of Nb in its +5 oxidation state in each of them, which was further confirmed by XPS analysis data.

3.3.2.1 SEM and EDX analysis

The changes in surface morphology of the polymeric resin at different stages of preparation of the pNb compounds are seen in SEM images presented in **Fig. 3.1**.

Comparison of the micrographs revealed that the fairly even surface of the pure polymer was distinctly altered after functionalization with the amino acid (**AA**) ligands. Grafting of the peroxidoniobium species to the resin resulted in further modification of the surface topography, as randomly oriented depositions of pNb species on the external surface of the complexes could be clearly seen in the micrographs (**Fig. 3.1**).

The energy dispersive X-ray (EDX) analysis data further showed Nb, in addition to C, N, O, and Na as constituents of the complexes (**Fig. 3.2**, **Table 3.1**). The EDX analysis, which provides *in situ* chemical analysis of the bulk, was carried out by focusing multiple regions on the compound surface. The EDX data agreed well with the elemental analysis values.
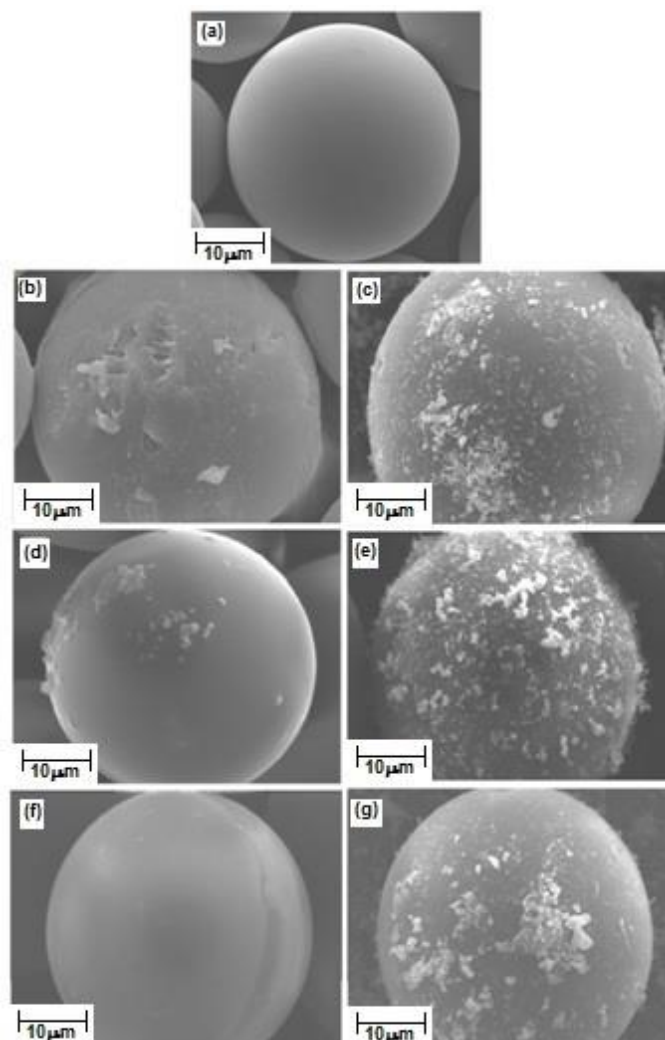

Fig. 3.1 Scanning electron micrographs of (a) **MR**, (b) **MRV**, (c) **MRVNb** (**3.1**), (d) **MRN**, (e) **MRNNb** (**3.2**), (f) **MRG** and (g) **MRGNb** (**3.3**).

Table 3.1 Analytical data of the complexes **3.1-3.3**

| Compound	% found from elemental analysis (% obtained from EDX spectra)						%O_2^{2-}	Nb: O_2^{2-}	Metal loading[a] (mmol g^{-1} of polymer)
	C	H	N	Na	Cl	Nb			
MRV	73.42	6.92	1.32	-	-	-	-	-	-
	(73.12)	-	(1.56)	-	(1.63)	-	-	-	-
MRVNb	58.54	5.44	2.75	-	-	-	-	-	-
	(58.18)	-	(2.96)	(7.68)	(0.65)	(2.77)	2.57	1:3	0.30
MRN	65.72	6.68	1.16	-	-	-	-	-	-
	(65.93)	-	(1.24)	-	(1.03)	-	-	-	-
MRNNb	45.23	5.61	1.13	-	-	-	-	-	-
	(44.99)	-	(1.36)	(10.16)	(0.58)	(3.33)	3.38	1:3	0.36
MRG	61.97	6.59	1.08	-	-	-	-	-	-
	(62.11)	-	(1.12)	-	(2.01)	-	-	-	-
MRGNb	41.11	6.54	1.24	-	-	-	-	-	-
	(41.80)	-	(1.42)	(12.63)	(0.92)	(2.49)	2.32	1:3	0.27

[a]Metal loading $= \dfrac{\text{Observed metal \% X 10}}{\text{Atomic weight of metal}}$
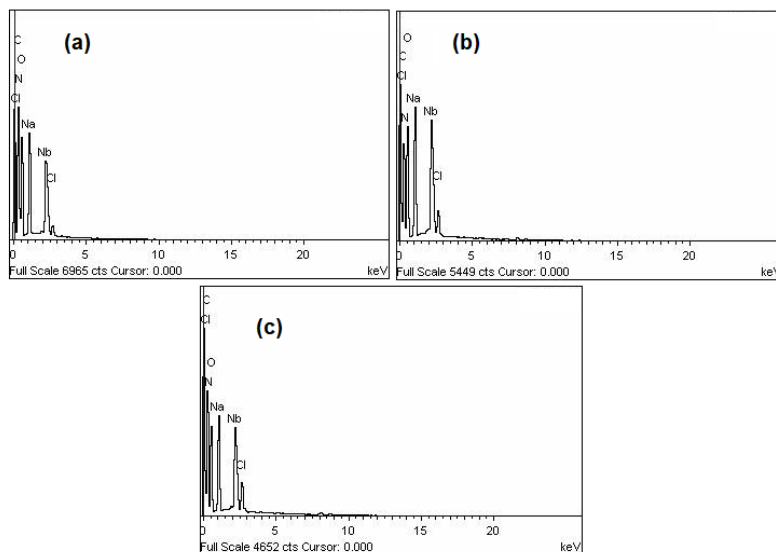
Fig. 3.2 EDX spectra of (a) **MRVNb** (**3.1**), (b) **MRNNb** (**3.2**) and (c) **MRGNb** (**3.3**).

3.3.2.2 Powder X-ray diffraction studies

The powder X-ray diffraction analysis of the peroxidoniobium compounds **3.1-3.3**, and the host resin has been performed in the range of 2θ values of 10 to 70º (**Fig. 3.3**). The diffractogram of PS-DVB resin displayed the typical broad diagnostic diffraction peak centered at the 2θ value of *ca*. 20° [**Fig. 3.3**(a)] [56,57]. After anchoring of the pNb species,
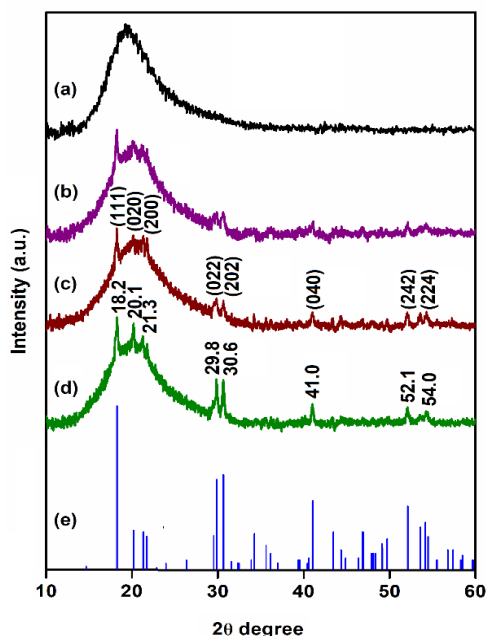
**Fig. 3.3** XRD patterns of (a) **MR**, (b) **MRVNb** (**3.1**), (c) **MRNNb** (**3.2**), (d) **MRGNb** (**3.3**), and (c) reference powder X-ray diffraction pattern of Na_3NbO_8 (JCPDS code 52-0708).

the position of this peak has been retained in the diffractograms of the compounds [**Fig. 3.3** (b-d)], indicating that the structure of the polymer resin has been preserved in the compounds. The diffraction patterns of the polymeric complexes showed additional peaks at 2θ values of *ca.* 18.2, 20.1, 21.3, 29.8, 30.6, 41.0, 52.1, and 54.0°, which resembled the pattern observed for peroxidoniobium species (PDF reference code 52-0708) due to planes (111), (020), (200), (022), (202), (040), (242), and (224), respectively. These observations indicated the attachment of the pNb species to the polymer matrix leading to the generation of the supported Nb compounds.

3.3.2.3 X-ray photoelectron spectroscopy

The XPS spectra of the compounds (**Fig. 3.4**) exhibited the characteristic well-resolved components of $3d_{5/2}$ and $3d_{3/2}$ doublet for niobium at binding energy (BE) of 207.0 and 209.7 eV, respectively. The values correspond to the typical binding energy (BE) data for Nb in +5 oxidation state [58,59]. The successful anchoring of Nb(V) to the pendant ligands of the functionalized resin has been further proved by peaks appearing at BE values characteristic of oxygen, nitrogen and carbon. Thus, XPS analysis results testified to the presence of peroxidoniobium(V) species on the surface of the complexes.
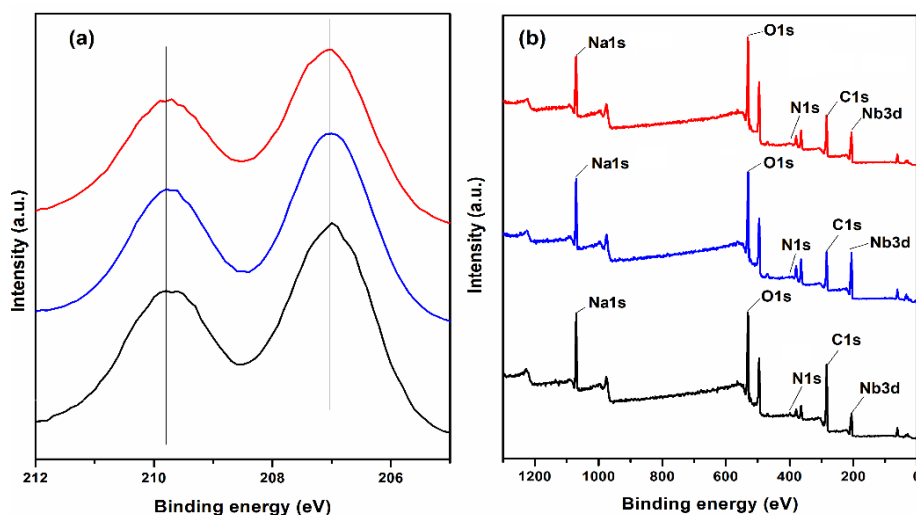
Fig. 3.4 (a) XPS spectra of Nb ($3d_{5/2}$) and ($3d_{3/2}$) and (b) XPS survey spectra for the compounds. **"Black line"** represents **MRVNb (3.1), "**Blue line**"** represents **MRNNb (3.2)** and "Red line" represents **MRGNb (3.3)**.

3.3.2.4 BET analysis

The changes occurring in the textural properties of the polymers during the course of preparation of the immobilized complexes **3.1-3.3** were investigated employing BET

analysis with nitrogen adsorption method [60]. It has been observed that after grafting of the ligands on the resin and subsequent anchoring of the Nb complexes, a consistent decrease in surface area of the polymer samples occurred in all the complexes. Functionalization of **MR** led to a reduction in specific surface area (S_{BET}) from 11.5 (pure resin) to 8.6, 9.6 and 1.8 m^2g^{-1} for **MRV**, **MRN**, and **MRG**, respectively. The specific surface area was further reduced to 2.6, 8.7 and 0.7 m^2g^{-1} for Nb anchored compounds **MRVNb** (**3.1**), **MRNNb** (**3.2**), and **MRGNb** (**3.3**), respectively. It has been well documented that the incorporation of metal complexes onto supports results in reduction in specific surface area of the supporting material [26,48,49,61-63].

3.3.2.5 FTIR and Raman spectral analysis

The FTIR spectra of the immobilized complexes **3.1-3.3** along with the respective functionalized polymers are shown in **Fig. 3.5-3.7** and the complementary Raman spectra for the compounds are illustrated in **Fig. 3.8**. A comparative analysis of FTIR and Raman spectral data provided important evidences in support of the successful covalent anchoring of **AA** ligands to the host PS-DVB resin followed by coordination of peroxidoniobium, $[Nb(O_2)_3]^-$ moieties to the functionalized polymer. The empirical assignments are based on the existing literature.

The intense peak at 1264 cm^{-1} in the spectrum of virgin **MR** is typical of ν(C-Cl) mode of -CH_2Cl moiety [52,64]. Attachment of ligand to the **MR** is usually accompanied by disappearance or decrease in intensity of the ν(C-Cl) absorption in the IR as well as Raman spectra [52,64]. Clear indication of substitution of Cl^- from the -CH_2Cl group of the host resin by the ligands [52,64] was obtained from the near disappearance of the ν(C-Cl) band in the spectra of the functionalized resins **MRV**, **MRN**, and **MRG** [**Fig. 3.5-3.7**]. In addition, a new weak intensity band attributable to ν(C-N) appeared at *ca*. 1085 cm^{-1}, suggesting the formation of C-N linkage *via* replacement of Cl^- groups of the polymeric matrix by the amino acids [48,49,52,64].

The spectra of the complexes as well as the respective functionalized resin also displayed the expected absorptions typical of the host resin in the vicinity of *ca*. 3055, 2921, 1019, and 695 cm^{-1} corresponding to $\nu_{aromatic}$(CH), $\nu_{aliphatic}$(CH), $\delta_{aromatic\ in-plane}$(CH) and $\delta_{aromatic\ out-of-plane}$(CH) vibrations, respectively [48,49,52,64,65]. The valine and glycine
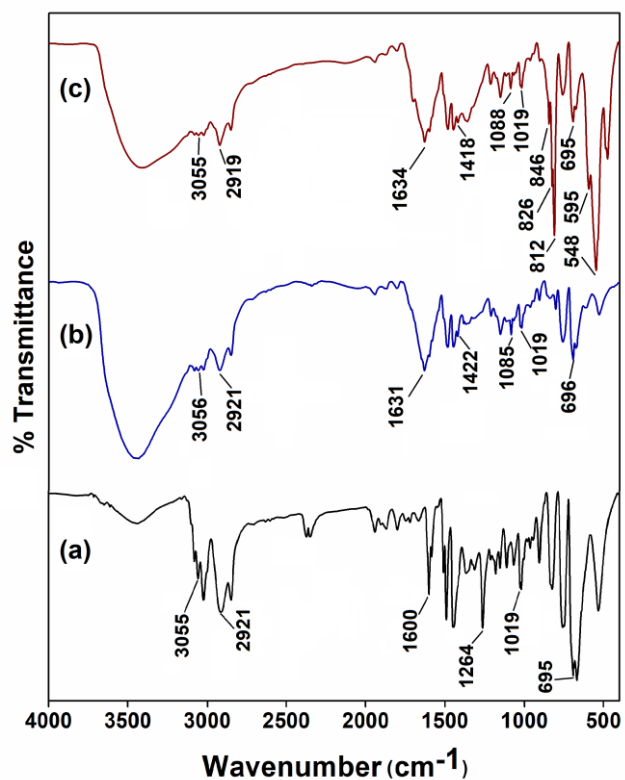
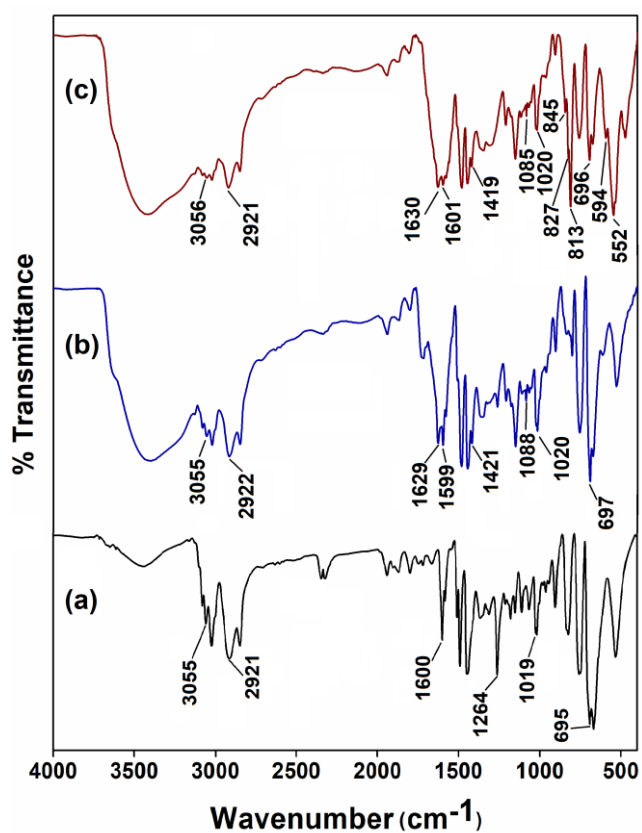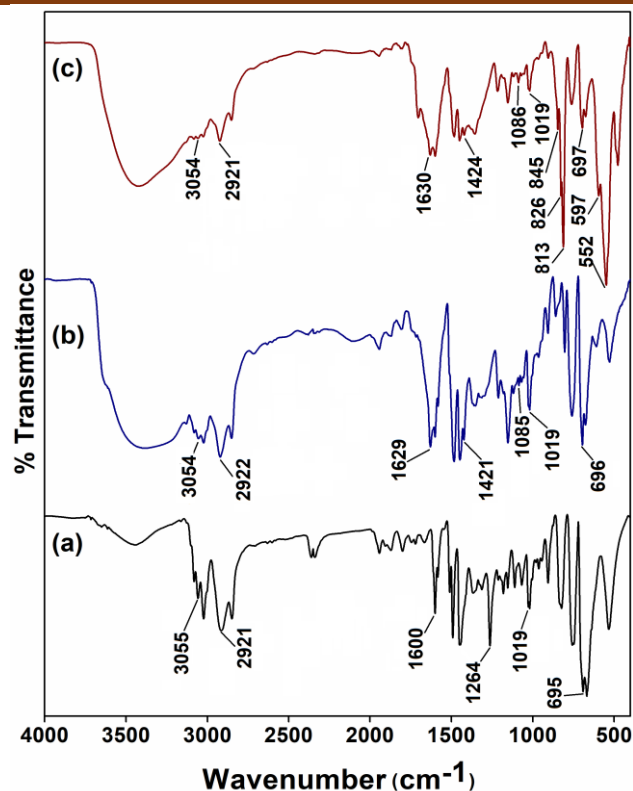**Fig. 3.5** FTIR spectra of (a) **MR**, (b) **MRV** and (c) **MRVNb** (**3.1**).

Fig. 3.6 FTIR spectra of (a) **MR**, (b) **MRN** and (c) **MRNNb** (**3.2**).

Fig. 3.7 FTIR spectra of (a) **MR**, (b) **MRG** and (c) **MRGNb** (**3.3**).

functionalized resins and the respective Nb anchored polymers **MRVNb** (**3.1**) and **MRGNb** (**3.3**) displayed carboxylate stretching ν_{asym}(COO) between 1630-1634 cm^{-1} region in the IR, as well as in the Raman spectra, whereas ν_{sym}(COO) vibration occurred in the 1418-1424 cm^{-1} region [65]. In the IR and Raman spectra of asparagine grafted polymer **MRN** and the respective compound **MRNNb** (**3.2**), bands due to ν_{asym} and ν_{sym} carboxylate stretching modes occurred in the 1598-1602 and 1421-1412 cm^{-1} region, respectively [66-68]. In the spectrum of **MRN** species, the strong IR band occurring at 1629 cm^{-1} has been attributed to ν(C=O) (amide I) mode, as amide I band usually appears as most intense absorption in the spectrum of asparagine [66-68]. From the unaltered position of this band in the spectrum of **3.2**, the possibility of participation of the side-chain amide group in metal binding could be ruled out. The IR spectra of the complexes indicated the presence of free -COOH groups by displaying a band in the 1703-1720 cm^{-1} region. The ν(NH) bands were difficult to distinguish with certainty as these vibrations overlapped with ν(OH) modes of lattice water.

Apart from the typical bands of the **AA** grafted polymeric support, the FTIR and Raman spectra of the complexes evidenced for the presence of [Nb(O$_2$)$_3$]$^-$ moiety in the

compounds by displaying diagnostic absorptions attributable to the ν(O-O) modes of η^2-peroxido group in the expected range of 800-900 cm^{-1} along with ν_{asym}(Nb-O$_2$) and ν_{sym}(Nb-O$_2$) bands in the 500-600 cm^{-1} region [54,69,70]. Importantly, both IR and Raman spectral patterns of complexes **3.1-3.3** show three well-resolved ν(O-O) bands within the range of 800-900 cm^{-1}, in accordance with the empirical rule which states that presence of three ν(O-O) modes in the IR spectra indicates formation of triperoxidoniobium species [54,70]. The rule is also applicable to Raman spectroscopy [54,70].
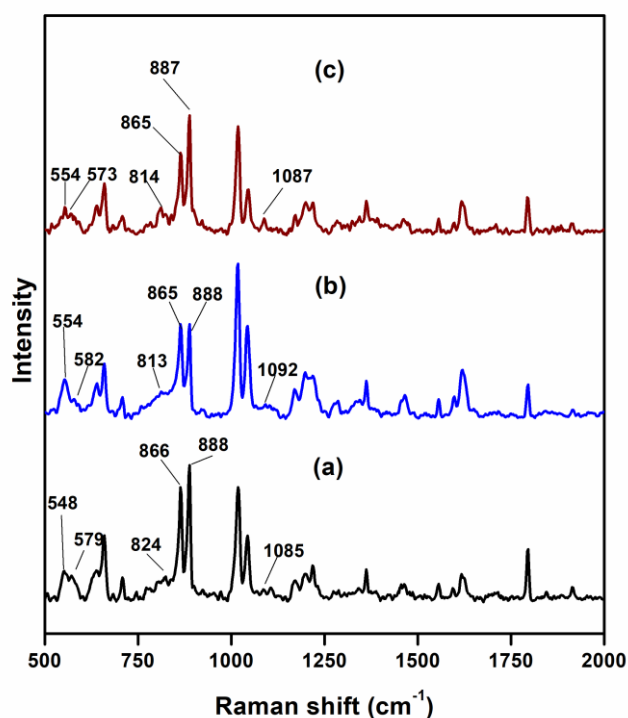
**Fig. 3.8** Raman spectra of (a) **MRVNb** (**3.1**), (b) **MRNNb** (**3.2**) and (c) **MRGNb** (**3.3**).

3.3.2.6 Electronic spectral studies

The diffuse reflectance UV-visible spectrum of each of the immobilized pNb compounds showed two bands within the 270-400 nm region as seen in **Fig. 3.9**. The intense band at around 270 nm has been assigned to the $\pi \rightarrow \pi^*$ transition in the polymer support [71,72]. The band occurring at around 380 nm is attributable to the peroxido ligand to the niobium metal (LMCT) charge transfer absorption, evidently originating from the anchored pNb complexes of the compounds [73,74].
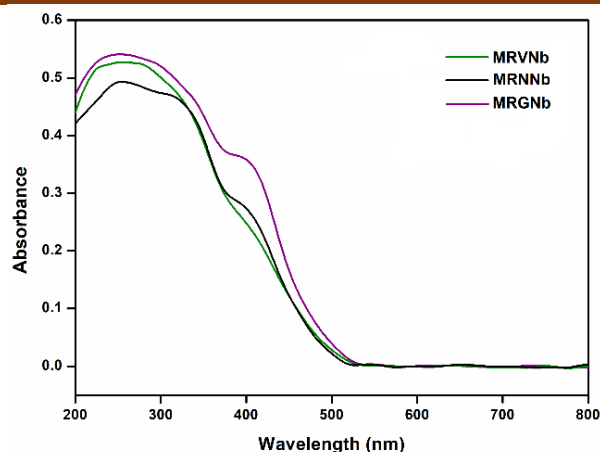
Fig. 3.9 Diffuse reflectance UV-visible spectra of **MRVNb**, **MRNNb** and **MRGNb**.

3.3.2.7 ^{13}C NMR analysis

The solid state ^{13}C NMR spectral resonances of the compounds and the respective **AA** grafted resins are shown in **Fig. 3.10-3.12**. The corresponding chemical shifts assigned based on the available literature [48,49,75-77], are provided in **Table 3.2**. A comparative evaluation of the NMR spectral data indicated modification of carbon signals to various extents after functionalization and subsequent metal anchoring. In addition to the expected signals of the base polymer belonging to quaternary aromatic, protonated aromatic, aliphatic methine, and -CH$_2$Cl group C atoms, spectra of the **AA** functionalized resins, **MRV**, **MRN**, and **MRG** showed several new resonances [76]. A well-resolved signal located at around 64 ppm indicated the presence of amine bound methylene C atom resulting from the substitution of Cl$^-$ by **AA** to form C-N bond [48,49,77]. The resonances corresponding to the chiral C atoms of the pendant **AA** ligands valine and asparagine, however, could not be resolved due to their merging with the significantly broad and intense peaks originating from the host polymer matrix. The carboxylate C resonance appeared in the vicinity of 184 ppm in the **AA** grafted polymer **MRV** and **MRG**. In the case of **MRN**, carboxylate and amide C resonances of asparagine were observed as two close signals at 181 and 179 ppm, respectively. The nearly unaltered chemical shift of amide C atom of **MRNNb** (**3.2**) at *ca.* 179 ppm indicated non-involvement of this group in metal coordination. A remarkable observation of the spectrum of each of the niobium loaded complexes, has been the appearance of a new peak at a much lower end of the field at *ca.* 210 ppm, along with the considerable weakening of the carboxylate carbon resonance at *ca.* 180 ppm. The low field signal at *ca.* 210 ppm is characteristic of C
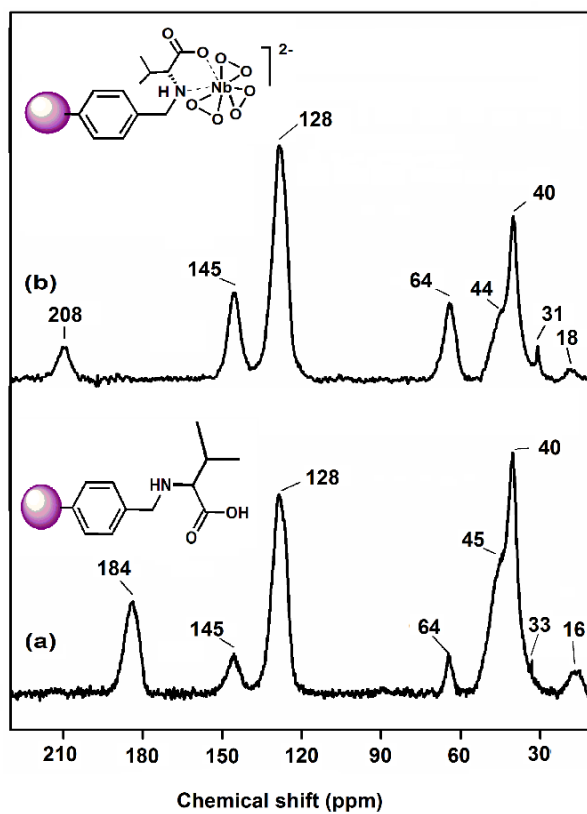
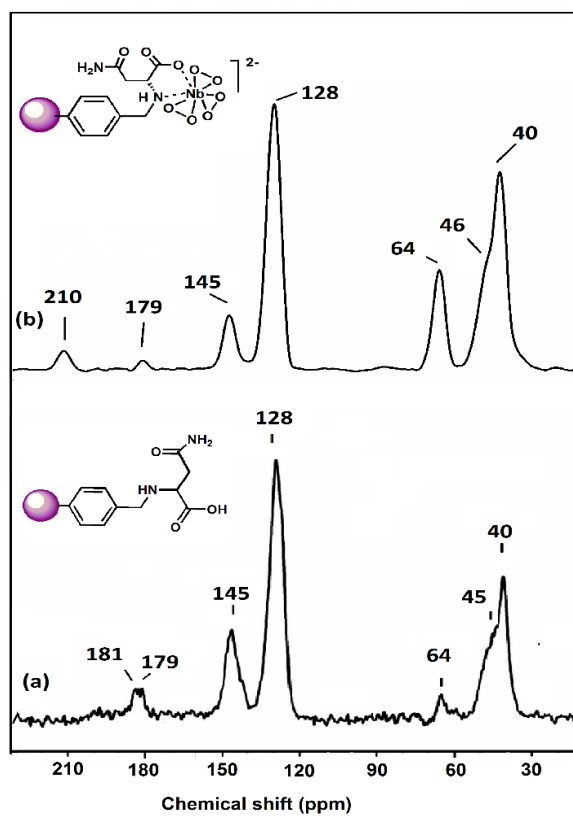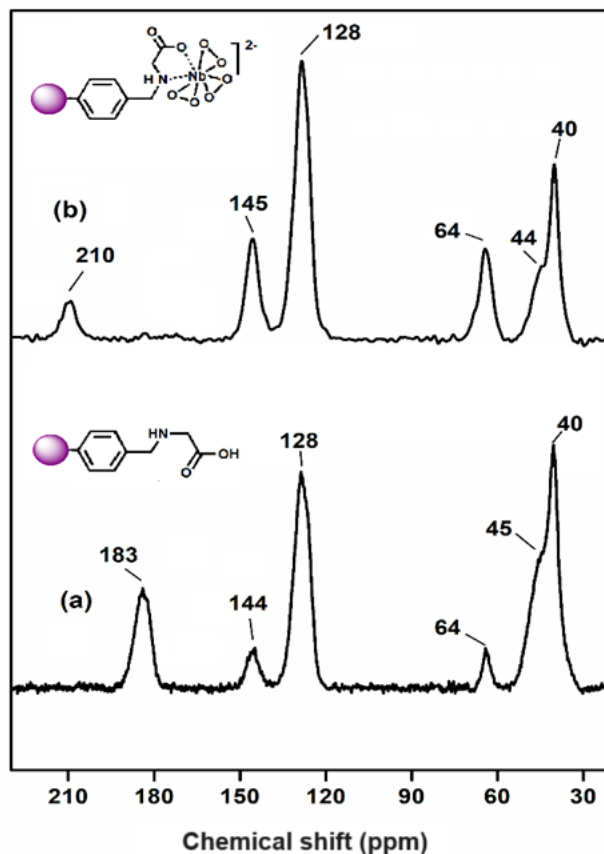**Fig. 3.10** ^{13}C NMR spectra of (a) **MRV** and (b) **MRVNb** (**3.1**).

Fig. 3.11 ^{13}C NMR spectra of (a) **MRN** and (b) **MRNNb** (**3.2**).

Table 3.2: ^{13}C N**MR** chemical shifts for **MR,** amino acid linked **MR** and polymer bound complexes

| Compound	Chemical shift (ppm)								
	Merrifield resin						Amino acid		
	Quaternary Aromatic Carbons	Protonated Aromatic Carbons	Aliphatic Methine Carbons	CH$_2$Cl	C-NH	CONH$_2$/CH$_3$	CH	Carboxylate	
								Free	Complexed
MR	145.18	128.36	41.04	46.17	-	-	-	-	-
MRV	145.79	128.48	40.52	45.81	64.34	16.93	33.52	184.10	-
MRVNb	145.81	128.64	40.23	44.52	64.35	18.36	31.03	-	208.83
MRN	145.51	128.66	40.47	45.61	64.30	179.89	-	181.59	-
MRNNb	145.58	128.61	40.39	46.02	64.30	179.18	-	-	210.24
MRG	144.97	128.69	40.52	45.61	64.14	-	-	183.72	-
MRGNb	145.72	128.49	40.01	44.30	64.50	-	-	-	210.63

Fig. 3.12 ^{13}C NMR spectra of (a) **MRG** and (b) **MRGNb** (**3.3**).

resonance of metal coordinated carboxylate group [48,49,55]. The observation signified anchoring of niobium to the polymer matrix *via* carboxylate groups of pendant **AA** ligands [78,79], which is in conformity with the mode of Nb coordination indicated by IR and Raman spectral results.

3.3.2.8 Thermogravimetric analysis

Thermograms of the peroxidoniobate anchored complexes **3.1-3.3** are shown in **Fig. 3.13** and the corresponding mass loss data are depicted in **Table 3.3**. All pNb loaded complexes, after releasing the water of crystallization below *ca*. 95 ℃, undergo degradation in the temperature range of *ca*. 105-175 ℃ which has been ascribed to the loss of coordinated peroxido complexes from the anchored $[Nb(O_2)_3]^-$ groups. The subsequent step of degradation has been observed in the temperature range of *ca*. 170-265 ℃ for the complexes due to the release of amino acid groups from the polymer support [80,81]. It is notable that the TGA of the pNb anchored compounds showed a close analogy with the respective amino acid grafted resin, *viz.*, **MRV**, **MRN**, or **MRG**, above the temperature of *ca*. 170 ℃. The polymeric compounds finally undergo a two-stage decomposition in the

temperature range of 280-700 ℃ due to the degradation of the remaining base polymer [82]. After complete degradation of the compounds, the remaining residue was subjected to IR spectral analysis. As anticipated, the residue was found to be oxidoniobium species along with char residue of the polymer.
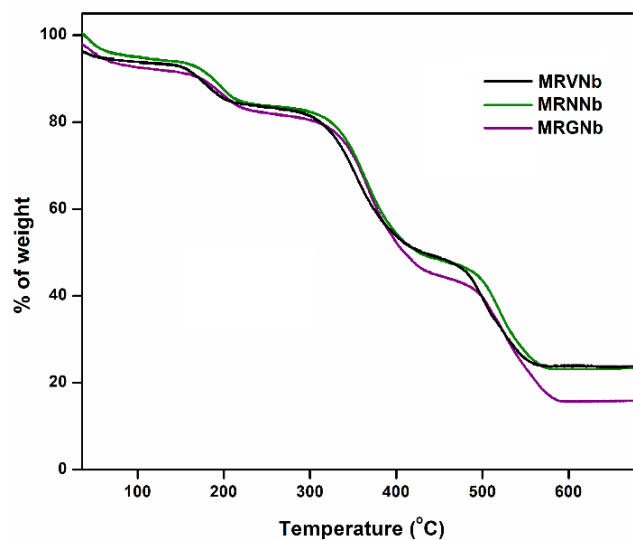
Fig. 3.13 Thermograms of the complexes **MRVNb, MRNNb** and **MRGNb**.

Table 3.3: TGA data for amino acid functionalized **MR** and metal-polymer complexes

Compound	Temperature range (°C)	Observed weight loss (%)	Final residue (%)
MRV	34-96	2.7	18.3
	154-235	12.3	
	267-698	66.7	
MRVNb	36-96	6.2	22.9
	104-169	2.2	
	171-253	8.7	
	263-454	35.4	
	457-698	24.6	
MRN	35-95	3.5	13.1
	148-257	12.5	
	263-698	70.9	

Continued…

| Compound	Temperature range (°C)	Observed weight loss (%)	Final residue (%)
MRNNb	37-94	5.7	23.5
	103-175	3.0	
	177-264	8.6	
	266-451	33.7	
	453-698	25.5	
MRG	34-97	2.8	11.7
	162-243	13.4	
	263-697	72.1	
MRGNb	26-95	6.4	17.8
	104-171	2.4	
	173-245	7.8	
	269-447	37.1	
	456-698	28.5	

Based on the aforementioned collective evidences, a structure representing polymer bound pNb complexes of the type illustrated in **Scheme 3.1** has been envisaged. The proposed structure of the catalytically active species can be depicted as a Nb(V) center with three η^2-peroxido groups bonded *via* carboxylate and -NH group of pendant **AA** ligand of the polymer. The side-chain amide group of asparagine which normally exists in the protonated form in the solution, does not usually participate in metal coordination [83-85]. Eight-fold coordination around Nb(V) center has been observed as a common feature in the reported structurally characterized pNb complexes [54,55,69,86].

3.3.3 Catalytic performances

3.3.3.1 Epoxidation of olefins

To evaluate the catalytic activity of the immobilized peroxidoniobium complexes, we chose to examine the oxidation of styrene with aqueous 30% H_2O_2 as a model reaction. Styrene being electron poor, its epoxidation over d^0 metal oxide catalysts usually provides low conversion and poor selectivity and thus is considered as a challenging reaction [25,33,87]. Apart from epoxide, which is known to be highly susceptible to ring-opening reaction [7,25,87], styrene oxidation usually yields benzaldehyde as an additional product

(**Scheme 3.2**). Strategically, screening of the reaction condition for the maximum transformation of styrene to the desired epoxide was the first task. As a starting point, we conducted experiments using complex **MRVNb** (**3.1)** as catalyst maintaining Nb: styrene molar ratio of 1:1000 and styrene: H_2O_2 ratio of 1:1 in absence of organic solvent.
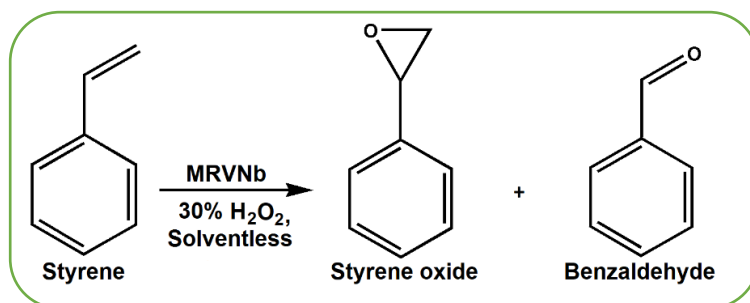
Scheme 3.2 Epoxidation of styrene by **MRVNb** (**3.1**).

We were pleased to find that the catalyst was highly active under these conditions as >92% styrene conversion could be achieved with the corresponding epoxide selectivity of >97% and turn over number (TON) value as high as 920 per Nb atom, using just stoichiometric amount of 30% H_2O_2. However, with 2 equivalents of H_2O_2, the reaction proceeded almost quantitatively to afford the desired epoxide with nearly 100% selectivity with a TON value of 990. Thus, styrene: H_2O_2 molar ratio of 1:2 was considered ideal in order to achieve reasonably good TON along with high epoxide selectivity.

We further probed the reaction with respect to catalyst loading, besides conducting a blank run in absence of the catalyst as shown in **Table 3.4** and **Fig. 3.14**. It is evident that increase in the amount of Nb loading resulted in an improvement of % conversion of styrene, but rendered a decrease in resultant TON value. Thus, the conversion versus catalyst profile (**Fig. 3.14**) revealed Nb: substrate molar ratio of 1:1000 to be optimal for the epoxidation. The vital role played by the catalyst in facilitating the oxidation is evident when the results obtained in presence of the catalyst were compared to poor % conversion afforded by the control run [**Table 3.4** (entry 4), **Fig. 3.14**]. The control run conducted in absence of the catalyst under otherwise identical reaction condition provided less than 10% conversion within the initial *ca.* 1.5 h of reaction time and no further conversion was noted even beyond 6 h. As the synthesized catalysts were formed by the substitution of one peroxido ligand from the neat precursor complex with the amino acid functionalized Merrifield resin, it was important to investigate the impact of such ligand replacement on catalytic activity of the peroxido compound $Na_3[Nb(O_2)_4]$ (**TpNb**). When the reaction was

conducted using free unsupported pNb complex $Na_3[Nb(O_2)_4]$ in lieu of the immobilized catalyst [**Table 3.4** (entry 5), **Fig. 3.14**] maintaining the same Nb loading, considerably lower conversion was obtained. These findings clearly indicate that the superior activity displayed by the catalyst originates from the immobilization of the peroxido-Nb complex on a polymer support. **Fig. 3.15** depicts the comparative conversion of styrene and epoxide selectivity shown by the immobilized catalysts **3.1-3.3** along with the free catalyst **TpNb** under the optimized reaction conditions.

**Table 3.4:** Effect of catalyst loading on styrene oxidation catalyzed by **3.1**[a]

Entry	Molar ratio (Nb:Sty)	Conversion (%)	Epoxide selectivity (%)	TON
1	1:500	99	≥99	495
2	1:1000	99	≥99	990
3	1:1500	75	≥97	1136
4[b]	-	9	≥95	-
5[c]	1:1000	47	≥92	470

[a]Reaction conditions: Styrene (5 mmol), 30% H_2O_2 (10 mmol, 1.13 mL), 80 °C, 6 h, without solvent. [b]Blank reaction without any catalyst. [c]Using $Na_3[Nb(O_2)_4] \cdot 13H_2O$ as catalyst (0.005 mmol of Nb).
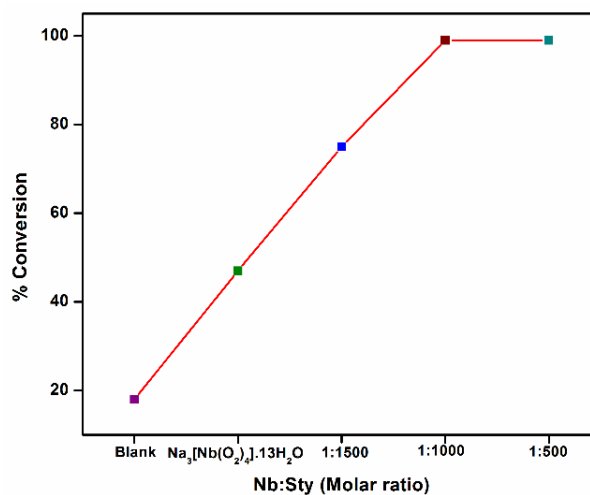
Fig. 3.14 Styrene conversion versus catalyst amount (Catalyst **3.1**). Reaction conditions: mentioned under **Table 3.4**.
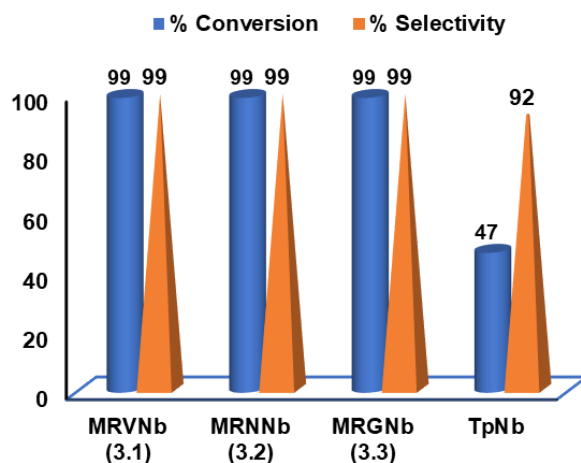
Fig. 3.15 Diagram depicting the conversion of styrene and epoxide selectivity shown by the polymer immobilized catalysts **3.1-3.3** along with the precursor complex, $Na_3[Nb(O_2)_4] \cdot 13H_2O$ (**TpNb**). [a]Reaction conditions: Styrene (5 mmol), catalyst (0.005 mmol of Nb), 30% H_2O_2 (10 mmol, 1.13 mL), 80 ℃, 6 h, without solvent.

The impact of the reaction temperature on the rate of the reaction is visible from the results presented in (**Table 3.5** and **Fig. 3.16**). Although a mere 2% conversion was obtained at room temperature [**Table 3.5** (entry 1), **Fig. 3.16**], on increasing the temperature to 60 ℃, styrene conversion leapt up to 64% [**Table 3.5** (entry 2), **Fig. 3.16**] affording >99% epoxide selectivity. A moderately elevated reaction temperature of 80 ℃ emerged to be favourable for achieving the maximum conversion of styrene [**Table 3.5** (entry 3), **Fig. 3.16**] without significantly affecting epoxide selectivity. Further increase in temperature up to 100 ℃ resulted in reduced conversion of styrene probably due to the degradation of H_2O_2 at a higher temperature [88].

Table 3.5: Effect of temperature on styrene oxidation by catalyst **3.1**[a]

Entry	Temperature (℃)	Conversion (%)	Epoxide Selectivity (%)	TON
1	RT	2	≥94	20
2	60	64	≥99	640
3	80	99	≥99	990
4	100	86	≥97	860

[a]Reaction conditions: Styrene (5 mmol), 30% H_2O_2 (10 mmol, 1.13 mL), catalyst **3.1** (0.005 mmol of Nb), 6 h, without solvent.
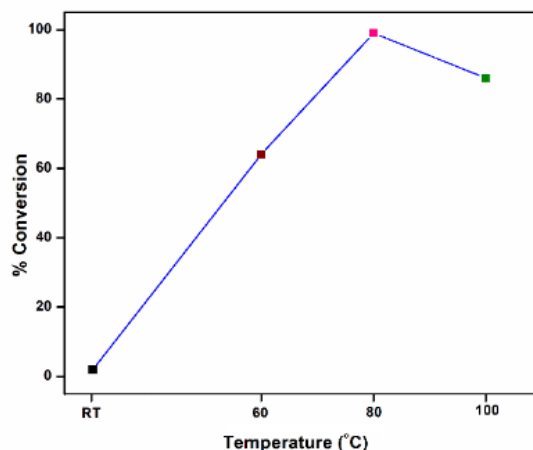
Fig. 3.16 Styrene conversion versus temperature (Catalyst **3.1**). Reaction conditions: as mentioned under **Table 3.5**.

The % conversion profile of styrene oxidation as a function of time, monitored over a span of 8 h, is illustrated in **Table 3.6** and **Fig. 3.17**. After the rapid oxidation occurring within the initial 2 h of starting the reaction to reach a conversion of >88%, a steady rise in styrene conversion was observed till *ca*. 6 h. It is notable that the reaction provided the highest initial turnover frequency (TOF) of approximately 640 h^{-1} within 30 min of starting the reaction with just 2 equivalents of H_2O_2 and 0.005 mmol Nb. Further extending the reaction time beyond 8 h, resulted only in a marginal increase in conversion and finally, it remained constant up to 24 h. This observation demonstrates that the catalyst

Table 3.6: Effect of reaction time on styrene oxidation with 30% H_2O_2 catalyzed by **3.1**[a]

| Entry	Time (h)	Conversion (%)	Epoxide Selectivity (%)	TON
1	0.5	32	≥95	320
2	1	38	≥95	380
3	2	88	≥98	880
4	3	93	≥99	930
5	5	98	≥99	980
6	8	99	≥99	990
7	24	99	≥99	990

[a]Reaction conditions: Styrene (5 mmol), 30% H_2O_2 (10 mmol, 1.13 mL), catalyst **3.1** (0.005 mmol of Nb, 16.7 mg), 80 ℃, without solvent.
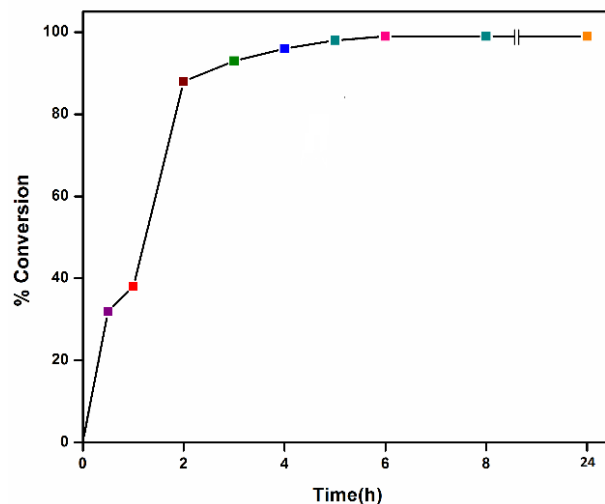
Fig. 3.17 Effect of time on styrene epoxidation. Reaction conditions: mentioned under **Table 3.6**.

is sufficiently robust to retain its activity, as well as selectivity even up to 24 h of reaction time, notwithstanding the elevated temperature at which the reaction was conducted. Importantly, we have also examined the scope of utilizing the procedure for scaled-up preparation and found that the established protocol could be applied at a ten-fold scale under optimized reaction conditions [**Table 3.7** (entry 1[d])].

In view of the encouraging results achieved in styrene oxidation, under organic solvent-free condition, we anticipated that the catalysts should efficiently catalyze the oxidation in any medium. The solid pNb catalysts **3.1-3.3** were insoluble and stable in aqueous, as well as organic solvents. Hence, the performance of the catalysts was investigated in water as well as in a variety of relatively safer halogen-free organic solvents as depicted in **Fig. 3.18**. It is evident that the reaction proceeded in each of the tested solvents with high epoxide selectivity. However, the best results in terms of conversion and TON, were obtained without using any solvent. Normally, reaction under solvent-free condition is faster than oxidation in presence of solvents, owing to higher substrate concentration. Importantly, the catalyst performed with greater efficiency in polar protic organic solvents and in fact, it displayed superior activity in aqueous medium. This finding is in accord with the previous literature on Nb-based catalysts showing promising catalytic performance in aqueous phase organic reactions due to their high stability towards metal leaching and hydrolysis [7,29,55,89].
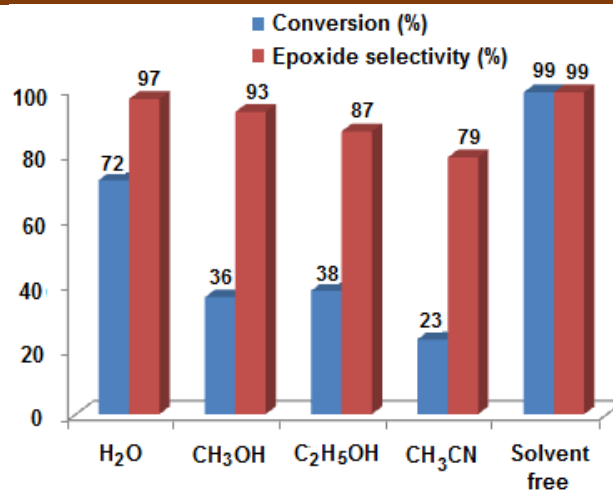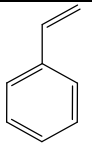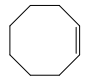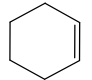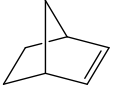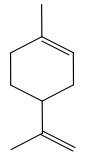
Fig. 3.18 Effect of solvent on styrene conversion. Reaction conditions: styrene (5 mmol), oxidant (10 mmol), catalyst **3.1** (0.005 mmol of Nb), solvent (5 mL), 80 °C, 6 h.

Having established the optimized reaction conditions for selective epoxidation of the model substrate styrene, a conjugated olefin, the catalysts **3.1-3.3** were evaluated for their activity in the selective epoxidation of a range of cyclic alkenes such as cyclohexene, cyclooctene and norbornene, as well as a cyclic unsaturated terpene, limonene. Our findings presented in **Table 3.7** demonstrate that each of the catalysts is active in the presence of hydrogen peroxide to afford high % conversion of the olefin to the desired epoxide. Clean conversion of cyclooctene to the corresponding epoxide could be accomplished with 100% selectivity, TON as high as 1000 per Nb atom within ≤1 h. Similarly, complete conversion of a bulky electron rich olefin norbornene, occurred with 97% epoxide selectivity (for catalyst **3.1**) within a reasonably shorter reaction time of 1.5 h [**Table 3.7** (entry 4)]. In case of cyclohexene, the oxidation was complete within just 30 min of reaction time at ambient temperature [**Table 3.7** (entry 3)]. The catalysts however displayed moderate selectivity towards cyclohexene epoxide, as the reaction led to the formation of other allylic oxygenated by-products such as cyclohexen-1-one and 2-cyclohexen-1-ol.

Epoxidation of terpenes such as limonene, a major constituent of several citrus oils, is an industrially significant chemical transformation as such epoxides are versatile building blocks for biodegradable polymers, as well as in the synthesis of pharmaceuticals, fragrances and food additives [20,37,90]. The oxidation of limonene usually yields both epoxidation and allylic oxidation products such as carveol and carvone, which are also of considerable commercial value [20,32,90,91]. In majority of cases 1,2-limonene epoxides

Table 3.7: Epoxidation of various alkenes with H_2O_2 catalyzed by compounds **3.1-3.3**[a]

Entry	Substrate	Time (h)	MRVNb (3.1)			MRNNb (3.2)			MRGNb (3.3)		
			% Conversion	% Epoxide Selectivity	TON	% Conversion	% Epoxide Selectivity	TON	% Conversion	% Epoxide Selectivity	TON
1		6	99	99[b]	990	99	99[b]	990	99	99[b]	990
		6	97[c]	99[b]	970	98[c]	99[b]	980	97[c]	99[b]	970
		6	99[d]	99[b]	990	99[d]	99[b]	990	99[d]	99[b]	990
2		0.75	100	100	1000	100	100[e]	1000	100	100[e]	1000
3		0.5	100[f]	39[g]	1000	100[f]	34[g]	1000	100[f]	44[g]	1000
4		1.5	100	97[h]	1000	100	91[h]	1000	100	94[h]	1000
5		8	93	63[i,j]	930	95	67[i,j]	950	91	74[i,j]	910

[a]All reactions were carried out with 5 mmol alkene, 10 mmol 30% H_2O_2, solvent-free, T = 80 °C, catalyst (0.005 mmol of Nb). [b]Other product: benzaldehyde. [c]% conversion for 5th reaction cycle. [d]% conversion of scaled-up reaction (5.7 g). [e]Reaction time: 1 h. [f]Reaction at room temperature. [g]Other products: 2-cyclohexen-1-one+2-cyclohexen-1-ol, [h]Other product: Norbornanone. [i]Limonene1,2-epoxide, [j]Other products: Carveol+Carvone.

are formed with high regioselectivity as the endo-cyclic double bond is more electron-rich compared to the exo-double bond, and thus is much more susceptible to epoxidation [20,32,37,90,91]. In the present study, polymer immobilized peroxidoniobium catalysts displayed noteworthy efficiency in promoting regioselective endocyclic epoxidation of limonene to yield 1,2-limonene epoxide as a predominant product (**Scheme 3.3**) with epoxide selectivity of *ca.* 70%, while other allylic oxygenated products carveol and carvone represented *ca.* 30% of the total yield (**Table 3.7**, entry 5). Interestingly, in case of limonene epoxidation over Nb-silicate catalysts, unusual preferential oxidation of the less electron-rich exocyclic C=C bond in limonene was also reported [26,32,33,37]. Although the exact cause of such unusual regioselectivity in limonene epoxidation over mesoporous Nb-SiO$_2$ are yet to be fully elucidated [32]. Ivanchikova *et al.* reported recently that such inversion of regioselectivity is mainly solvent-dependent [27,33]. Solvent-free conditions were not tested so far in Nb catalyzed limonene oxidations. Apparently, in case of the present catalytic system as the oxidations were conducted in absence of organic solvent, limonene epoxidation with H$_2$O$_2$ proceeds at more electron-rich 1,2 position as anticipated, to regioselectively form the endocyclic product.
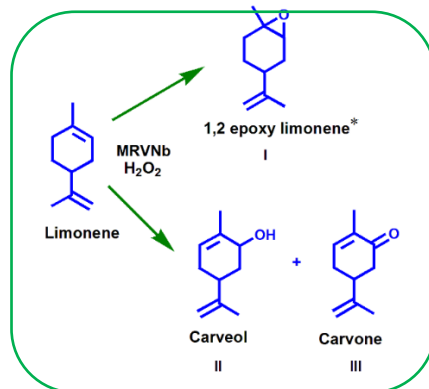
Scheme 3.3 Epoxidation of limonene with 30% H$_2$O$_2$ catalyzed by **MRVNb** (**3.1**) (*major product).

3.3.3.2 Oxidation of sulfides

Since each of the immobilized pNb catalysts efficiently facilitated the epoxidation of alkenes without organic solvent, we turned our attention towards extending the application of the catalysts to solvent-free oxidation of sulfides to sulfones. Details of the optimization study carried out using thioanisole (MPS) as a standard substrate are compiled in **Table 3.8**. An inspection of **Table 3.8** reveals that the best results in terms of

TON values without compromising the sulfone selectivity were obtained at room temperature by using catalyst: substrate molar ratio of 1:1000 and 2 equivalents of 50% H_2O_2, under solvent-free condition (**Table 3.8**, entry 3). Once again, results of a blank experiment without the catalyst, as well as the oxidation using neat pNb complex, $Na_3[Nb(O_2)_4]$ as a catalyst (**Table 3.8**, entries 9,10) provided low yield with poor selectivity, as has been observed in case of styrene epoxidation. These findings lend further credence to our observation regarding positive impact of heterogenization *via* polymer immobilization on the efficacy of the active peroxidoniobium complexes.

Table 3.8: Screening of reaction conditions for oxidation of thioanisole with 50% H_2O_2 catalyzed by **MRNNb** (**3.2)** under solvent-free condition[a]

Entry	Molar ratio (Nb:MPS)	H_2O_2 (equiv)	Time (min)	Isolated yield (%)	1a:1b	TON
1	1:1000	2[b]	180	97	44:56	970
2[c]	1:1000	2[b]	155	95	0:100	950
3	**1:1000**	**2**	**65**	**98**	**0:100**	**980**
4	1:1000	3	80	95	0:100	950
5	1:1000	4	90	97	0:100	970
6	1:2000	2	120	89	24:76	1780
7	1:500	2	45	95	0:100	475
8	1:100	2	20	97	0:100	97
9[d]	-	2	65	11	37:63	-
10[e]	1:1000	2	65	53	21:79	530

[a]All reactions were carried out with 5 mmol substrate, catalyst (0.005 mmol of Nb) at RT and without solvent. [b]Reaction with 30% H_2O_2. [c]Reaction at 80 °C with 30% H_2O_2. [d]Blank reaction without catalyst. [e]Reaction with $Na_3[Nb(O_2)_4]\cdot13H_2O$ as catalyst (0.005 mmol).

Apart from thioanisole, the standardized oxidation protocol could be applied to a wide range of structurally diverse organic sulfides to obtain the respective sulfones as the sole product. Appreciable turnover numbers and turnover frequencies obtained for all the substrates, as shown in **Table 3.9**, amply demonstrate the scope of the developed catalysts and the catalytic procedure. Each of the catalysts was found to be effective in oxidation and displayed comparable activity. Evidently, the type of the attached substituent influenced the rates of oxidation across the range of substrates investigated, as dialkylsulfides (**Table 3.9**, entries 2-4) manifested in faster oxidation whereas, conjugated less nucleophilic sulfides, *viz.*, vinylic, allylic, or aryl sulfides were oxidized at relatively slower rates. The observation is not unusual as H_2O_2 induced oxidation of thioethers has been known to occur through electrophilic addition of O atom [92,93].

Importantly, the catalysts exhibited outstanding chemoselectivity in the oxidation of sulfides containing additional functional groups susceptible to oxidation. Thus, the desired sulfone could be selectively obtained from allylic, vinylic, or alcoholic sulfides whereas, functional groups such as C=C bond or -OH group remained unaffected (**Table 3.9**, entry 8-10). In addition, similar to styrene epoxidation the sulfide oxidation also showed prospects for scaled-up applications as it could be effectively employed on a relatively larger scale (7.5 g of MPS) as seen from **Table 3.9** (entry 1[c]).

3.3.3.3 Heterogeneity test
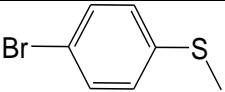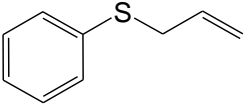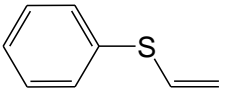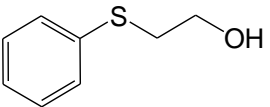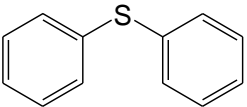
In order to confirm the heterogeneity of the developed catalytic oxidation processes, a standard hot filtration test was performed using styrene or MPS as substrate representing each type of oxidations, under optimized reaction conditions. As shown in the **Fig. 3.19**, the solid catalyst was removed from the reaction mixture after 90 min (25 min for MPS oxidation) of reaction time (at *ca*. 50 % of conversion) and the filtrate was allowed to react for further 6 h (for MPS, 1 h). No significant change in conversion in absence of the catalyst, indicated that the developed catalytic processes are truly heterogeneous in nature. The possibility of Nb species leaching out of the polymer support could further be ruled out, as the data obtained from the ICP-OES analysis of the filtrate did not indicate the presence of Nb in it.

Table 3.9: Selective oxidation of sulfide to sulfone with 50% H_2O_2 catalyzed by catalysts **3.1-3.3** at room temperature[a]

Entry	Substrate	MRVNb (3.1)			MRNNb (3.2)			MRGNb (3.3)		
		Time (min)	Isolated Yield (%)	TON	Time (min)	Isolated Yield (%)	TON	Time (min)	Isolated Yield (%)	TON
1		60	95	950	65	98	980	60	97	970
		60	95[b]	950	65	96[b]	960	60	97[b]	970
		60	96[c]	960	65	97[c]	970	60	96[c]	960
2		40	98	980	45	95	950	35	98	980
3		60	95	950	65	96	960	60	97	970
4		80	95	950	90	97	970	75	96	960
5		55	96	960	60	96	960	50	95	950
6		90	96	960	95	97	970	90	97	970

Continued…

Entry	Substrate	MRVNb (3.1)			MRNNb (3.2)			MRGNb (3.3)		
		Time (min)	Isolated Yield (%)	TON	Time (min)	Isolated Yield (%)	TON	Time (min)	Isolated Yield (%)	TON
7	Br—⬡—S—CH₃	80	97	970	85	95	950	75	96	960
8	⬡—S—allyl	140	94	940	145	97	970	135	95	950
9	⬡—S—vinyl	315	95	950	325	93	930	315	92	920
10	⬡—S—CH₂CH₂OH	205	98	980	210	97	970	200	96	960
11	⬡—S—⬡	260	92	920	270	94	940	250	95	950

[a]All reactions were carried out with 5 mmol substrate, 10 mmol 50% H_2O_2, catalyst (0.005 mmol of Nb) at room temperature and without solvent.

[b]% conversion for 5th reaction cycle. [c]Scale-up data (7.5 g of MPS).
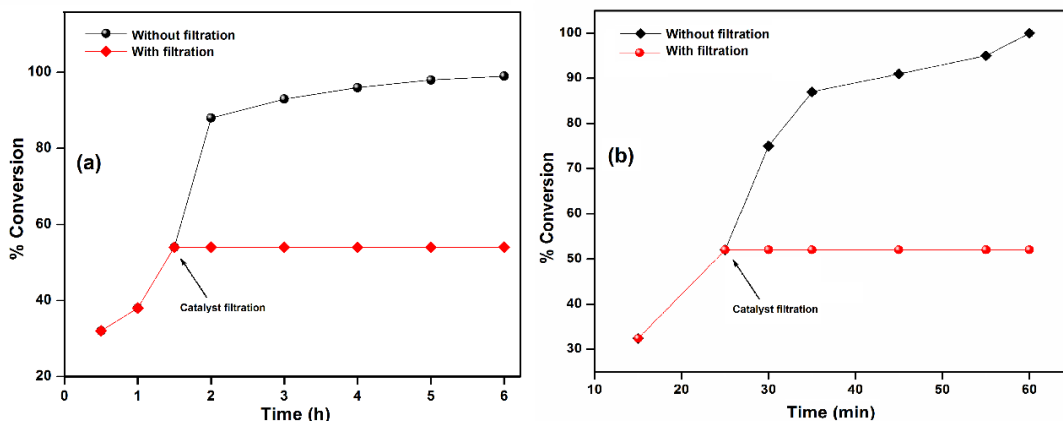
Fig. 3.19 Heterogeneity test for (a) styrene and (b) MPS.

3.3.3.4 Recyclability of the catalysts

For the practical utility of a catalytic process, from both economic and ecological standpoint, the stability and reusability of catalysts are of key importance. The solid catalysts could be easily separated by simple filtration or centrifugation after completion of the reaction, due to their heterogeneous nature. The recovered catalyst was washed with acetone, dried under vacuum, and then used in a fresh reaction run without further conditioning. Results presented in **Table 3.7** (entry 1[c]) and **Table 3.9** (entry 1[b]) and **Fig. 3.20** demonstrate impressive recyclability of the catalysts over at least five consecutive catalytic cycles in both types of transformations, *viz.*, the oxidation of olefins as well as sulfides, without any significant alteration in their selectivity.
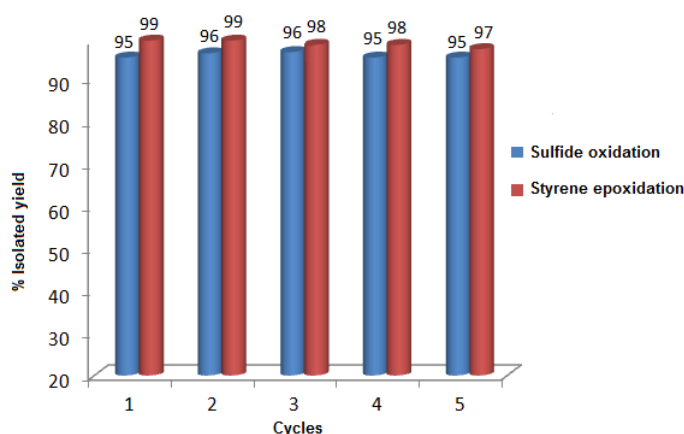
Fig. 3.20 Reusability of Catalyst **3.1** for selective oxidation of sulfide and styrene.

In order to further confirm the stability of the catalysts, the recovered catalysts were characterized by FTIR and EDX spectral studies. The FTIR spectra (**Fig. 3.21**) of the used

catalysts were found to be nearly identical with those of the fresh catalysts. Moreover, no quantitative loss in Nb content was indicated by EDX analysis results (**section 3.2.6**) compared to fresh catalyst. The findings further testify to the inherent stability of the catalysts evidently resulting from the strong attachment of the pNb species to the amino acid ligands of the polymer support.
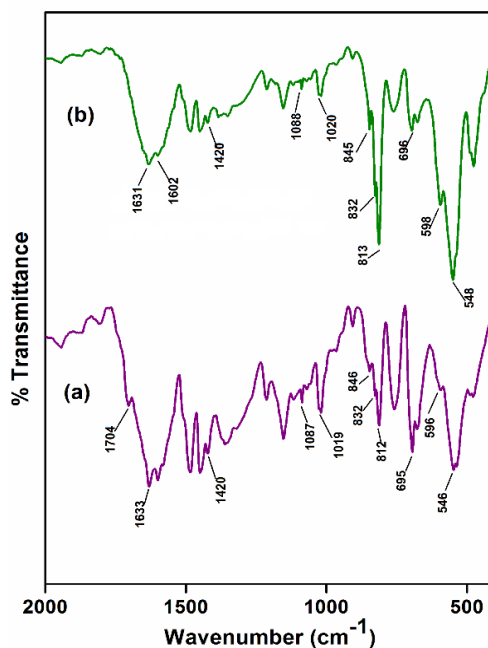
Fig. 3.21 FTIR spectra of (a) Catalyst **3.1** and (b) Catalyst **3.2** after 5th catalytic cycle.

3.3.3.5 H_2O_2 utilization efficiency

Assessment of the utilization efficiency or effective use of hydrogen peroxide in the oxidation process is of vital importance as it is evident from the literature that many of the transition metal catalysts decompose H_2O_2 at higher temperature or lower pH [94,95]. H_2O_2 utilization efficiency is defined as ($100 \times$ mole of H_2O_2 consumed in the formation of oxy-functionalized products/mole of H_2O_2 converted) [96]. In our present work, H_2O_2 utilization efficiency of styrene epoxidation was found to be remarkably high being within the range of (92-97%) in presence of the pNb catalysts. Similarly, oxidation of sulfides to sulfone also occurred with very high utilization efficiency of H_2O_2 with the efficiency percentage ranging between 95-98 % for the catalysts.

3.3.3.6 Comparison with some reported catalysts

As seen from the comparative report presented in **Table 3.10**, the catalytic activity reported here is comparable to or better than several recently reported niobium oxide-based

systems which were carried out in presence of various organic solvents [7,24-27,30,32,33, 35-38,40,87,91]. Under our non-solvent conditions, we have achieved outstanding results particularly in case of epoxidation of styrene, cyclooctene as well as norbornene. Notwithstanding the excellent selectivity of cyclooctene epoxide achieved with most of the reported Nb catalysts [24,30,33,35,36,38,50], the reactions provided moderate cyclooctene conversion [24,33,35,36,38], except in few cases [30,50]. Interestingly, 100% epoxide selectivity for cyclooctene was also obtained under non-solvent condition over Nb-MCM-41 catalyst, however the conversion was *ca.* 65% after 24 h and TBHP was used as the oxidant [24]. It is notable that, we are yet to come across any report on solvent-free epoxidation of substrates such as styrene, norbornene, or limonene catalyzed by heterogeneous Nb-based systems. With respect to limonene oxidation, a number of reported Nb catalysts yielded high conversion of limonene with excellent regioselectivity (>98%) to form monoepoxides [26,32,37]. However, the product obtained in most cases comprised of both endocyclic and exocyclic isomers [26,32,37,91]. On the other hand, the present polymer immobilized pNb catalysts, provided 95% limonene conversion with impressive regioselectivity to yield exclusively 67% endocyclic epoxide.

It is also significant to note that, for recyclability of most of the reported Nb-silica based catalysts, the recovered solid catalysts were often required to be calcined for restoration of catalytic activity for subsequent runs [26,32,35]. Moreover, recently reported catalyst $HNb(O_2)W_5/CNTs$ required to be pre-treated with $HClO_4$ prior to its re-use in second and subsequent runs [50]. Thus, a significant advantage offered by the present polymer immobilized peroxido-Nb catalysts is the ease of recovery and reusability for multiple catalytic cycles. Moreover, our conditions appear to be milder and eco-friendly as the present catalytic system offered selective epoxidation reactions with H_2O_2 as oxidant under solventless condition. Most importantly, all transformations in the present study, *viz.*, epoxidation, as well as sulfide oxidation were conducted at the natural pH of the reaction medium without using any acid, co-catalyst, or other non-green additives.

In order to rationalize the high activity and selectivity of the newly developed catalysts systems, it is relevant to recall the previous literature pertaining to the activity of heterogenized metal catalysts supported on organic polymers [43,97]. It has been observed that usually better catalytic activity and selectivity of the polymer immobilized catalysts are obtained with low loading of metal complexes for maximum site isolation of catalytic centers. Moreover, metal complexes should be attached to the polymer by a single flexible

Table 3.10: Activity of catalyst **3.1** in epoxidation of olefins *vis-à-vis* some reported heterogeneous Nb-based catalysts

Entry	Catalyst	Substrate	Catalyst amount	Reaction conditions	% Conversion/ % Selectivity	Ref
1	**MRVNb (3.1)**	**Styrene**	**0.005 mmol**	**6 h, 80 °C, H$_2$O$_2$, Solventless**	**99/99**	**This work**
2	Calix-Nb-SiO$_2$	Styrene	0.00102 M	6 h, 65 °C, H$_2$O$_2$, MeCN	53/20	25
3	Nb-KIT-5(10)	Styrene	20 mg	6 h, 50 °C, H$_2$O$_2$, MeOH	51/13	87
4	Nb-MMM-E	Styrene	0.005 mmol	1 h, 50 °C, H$_2$O$_2$, MeCN	20/50	33
5	**MRVNb (3.1)**	**Cyclooctene**	**0.005 mmol**	**45 min, 80 °C, H$_2$O$_2$, Solventless**	**100/100**	**This work**
6	Nb-MCM-41	Cyclooctene	1.04×10^{-5} mol	24 h, 90 °C, TBHP, Solventless	64.8/100	24
7	Nb-MMM-E	Cyclooctene	0.005 mmol	2 h, 50 °C, H$_2$O$_2$, MeCN	40/>99	33
8	Nb$_2$O$_5$-SiO$_2$	Cyclooctene	30 mg	5 h, 90 °C, H$_2$O$_2$, MeOH	61/100	35
9	Nb-MCM-41	Cyclooctene	100 mg	10 h, 80 °C, TBHP, Cyclohexane	19/95	38
10	Nb-SBA-15	Cyclooctene	0.1 g	48 h, 80 °C, TBHP, Ethyl acetate	80.5/99	30
11	HNb(O$_2$)W$_5$/CNTs	Cyclooctene	10 mg	1.5 h, 50 °C, H$_2$O$_2$, DMC	94/98	50
12	Nb$_2$O$_5$–SiO$_2$	Cyclooctene	600 mg	5 h, 70 °C, H$_2$O$_2$, MeOH	39.5/100	36

linkage in order to make the catalytic sites freely accessible [43,97]. It is therefore reasonable to expect that in the present case too, factors such as anchoring of the active peroxide-Nb complexes to the pendant ligand of the polymer *via* flexible coordination, as well as the low metal loading in the catalysts would facilitate site isolation effect which can induce increased activity and selectivity of the catalysts.
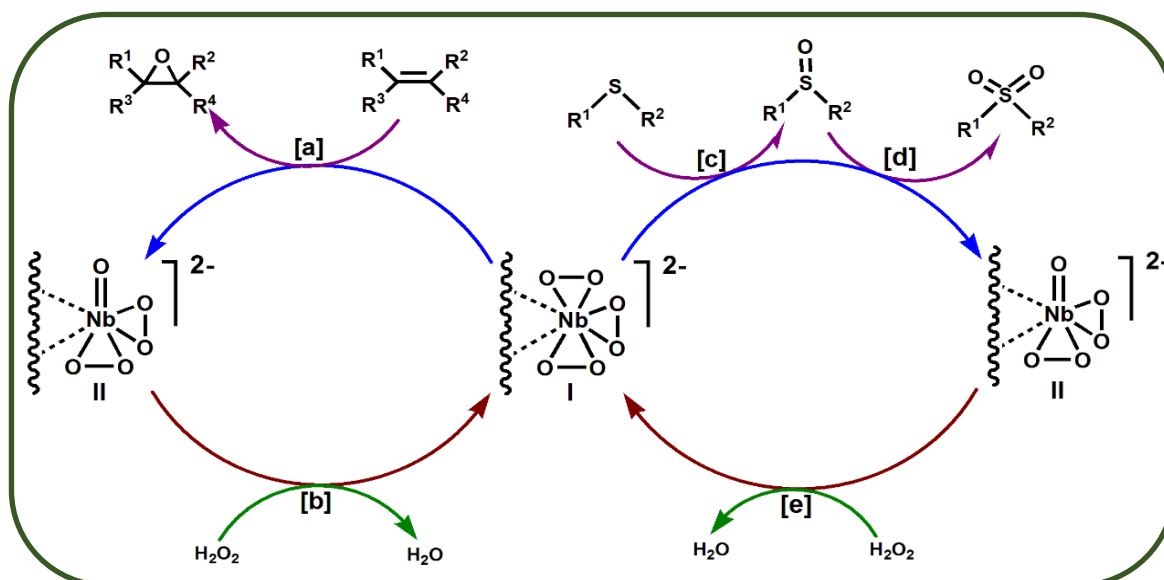
3.3.3.7 The proposed catalytic cycle

The mechanism of oxygen transfer to nucleophilic substrates from peroxido complexes of d^0 transition metal ions such as V(V), Mo(VI) and W(VI), has been extensively studied over the past decades. One of the widely accepted olefin epoxidation pathways involves a simple bimolecular interaction between the nucleophile and peroxidometal complex, leading to direct transfer of electrophilic oxygen of the metal-bound peroxido group to the alkene, through the formation of a three-membered ring transition state [98-101]. However, there is a paucity of information on mechanism of action of pre-formed Nb(V)-peroxido compounds in catalytic organic oxidations [102,103]. Nevertheless, the mode of liquid phase oxidation of olefins with H_2O_2, catalyzed by heterogeneous Nb-oxide based systems, have been investigated in recent years [27,104,105]. A range of oxidizing species were proposed to be involved as active intermediates including hydroperoxo, NbOOH [31,50,103,104] and *in situ* generated $Nb(\eta^2\text{-}O_2)$ species [27,106,107].

Keeping in view the above information, and based on the results of our present work, a catalytic cycle for olefin oxidation with H_2O_2, mediated by polymer-supported triperoxidoniobium complexes has been proposed (**Scheme 3.4**). The active Nb bound peroxido group of the pNb anchored catalyst is likely to transfer its electrophilic oxygen to the alkene (**reaction a**) to yield the corresponding epoxide. The epoxidation reaction is accompanied by the generation of oxidodiperoxidoniobium intermediate **II**. In the next step (**reaction b**), intermediate **II** reacts with H_2O_2 to regenerate the starting catalyst **I,** thereby leading to the formation of a catalytic cycle. In case of the oxidation of sulfide to sulfone, the reaction has been known to proceed *via* the formation of sulfoxide in a two-step catalytic process [48,55,108,109]. Accordingly, a plausible catalytic cycle envisaged for selective oxidation of sulfides to sulfone is shown in **Scheme 3.4** (**reactions c-e**).

There have been a number of reports documenting the formation of an oxidoperoxidoniobium(V) intermediate during the course of oxygen transfer from a pNb

species to a substrate [54,55,89,102,103,110]. In our previous work dealing with sulfide oxidation catalyzed by heteroleptic triperoxidoniobium complexes, our group could establish the identity of the intermediate species as a diperoxido-Nb(V) complex by isolating it into solid state [55]. With an aim to derive information on the proposed pathway for olefin oxidation in the present study, we have attempted to confirm the involvement of such an intermediate (species **II**) *via* its isolation and characterization. Taking a cue from our past experience [55], in order to isolate species **II**, we have conducted styrene oxidation using compound **3.1** as stoichiometric oxidant, instead of the terminal oxidant H_2O_2. Under these conditions, complete conversion of styrene to epoxide occurred within *ca*. 4 h of contact time. The solid product recovered from the spent reaction mixture was subsequently characterized by elemental and FTIR spectral analyses. Formation of a diperoxido-Nb species was clearly indicated by the 1:2 ratio for Nb: peroxide ligand obtained from elemental analysis data. The IR spectral changes (**Fig. 3.22**) furnished further evidence showing two distinct ν(O-O) bands at 852 and 805 cm^{-1} typical of diperoxido-Nb complex [70], instead of the three ν(O-O) absorptions of the starting triperoxidoniobium catalyst (**Fig. 3.5, 3.22**). Nearly unaltered positions of the IR bands due to the amino acid ligands of the host resin, demonstrated that the catalyst remained intact during the process of oxidation. Although we do not have further data to discuss the detailed mechanism, the above observations lent credence to the proposed catalytic cycle.

Scheme 3.4 Proposed catalytic cycles for epoxidation of olefins and oxidation of sulfides to sulfones. "〰" represents polymer chain.
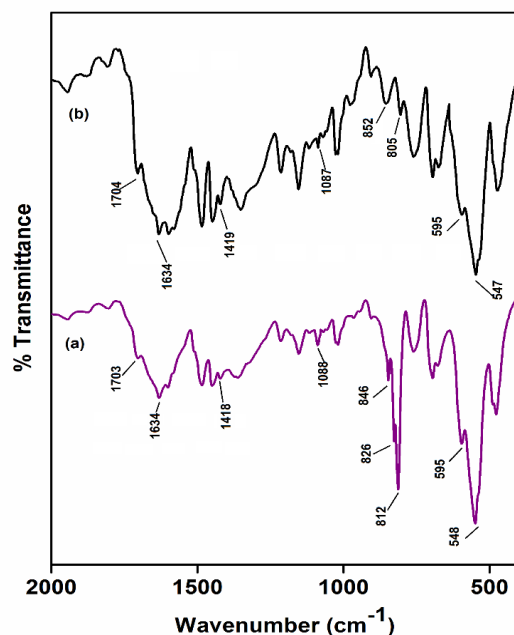
Fig. 3.22 IR spectra of (a) **MRVNb** (**3.1**) and (b) Diperoxidoniobate complex recovered after oxidation of styrene by Catalyst **3.1**, in absence of H_2O_2.

3.4 Conclusions

The present work demonstrated that, it is possible to generate simple, yet highly effective heterogeneous oxidation catalysts by grafting peroxidoniobium species on appropriately functionalized cross-linked PS-DVB resin. The novelty of the contribution lies in demonstrating remarkably enhanced activity of the immobilized pNb catalysts in the selective epoxidation of a variety of alkenes as well as oxidation of sulfides to the desired sulfones with excellent yield, TON as well as high H_2O_2 utilization efficiency. The transformations were achieved by employing H_2O_2 as green oxidant, under environmentally clean, solvent-free conditions. Facile and quantitative recoverability of the catalysts with no significant loss in product selectivity are important attributes of the present catalytic strategies. Importantly, the procedures offer the advantages of safety and ease of handling, as the catalysts were prepared employing a biologically inert, non-toxic transition metal and commercially available environmentally safe starting materials. In summary, in comparison to many other sophisticated supported catalytic systems, the developed pNb catalysts and the methodologies are characterized by simplicity along with efficiency, versatility and sustainability.

References

1. Noyori, R., Aoki, M., and Sato, K. Green oxidation with aqueous hydrogen peroxide. *Chemical Communications*, (16):1977-1986, 2003.

2. Sato, K., Aoki, M., and Noyori, R. A" green" route to adipic acid: Direct oxidation of cyclohexenes with 30 percent hydrogen peroxide. *Science*, 281(5383):1646-1647, 1998.

3. Sharma, A. S., Sharma, V. S., Kaur, H., and Varma, R. S. Supported heterogeneous nanocatalysts in sustainable, selective and eco-friendly epoxidation of olefins. *Green Chemistry*, 22(18):5902-5936, 2020.

4. De Faveri, G., Ilyashenko, G., and Watkinson, M. Recent advances in catalytic asymmetric epoxidation using the environmentally benign oxidant hydrogen peroxide and its derivatives. *Chemical Society Reviews*, 40(3):1722-1760, 2011.

5. Roberts, S. M. and Whittall, J. *Regio- and Stereo-Controlled Oxidations and Reductions*. Wiley-Interscience, New York, 2007.

6. Bauer, K., Garbe, D., and Surburg, H. *Common Fragrance and Flavor Materials: Preparation, Properties and Uses*. John Wiley & Sons, 2008.

7. Yan, W., Zhang, G., Yan, H., Liu, Y., Chen, X., Feng, X., Jin, X., and Yang, C. Liquid-phase epoxidation of light olefins over W and Nb nanocatalysts. *ACS Sustainable Chemistry & Engineering*, 6(4):4423-4452, 2018.

8. Caron, S., Dugger, R. W., Ruggeri, S. G., Ragan, J. A., and Ripin, D. H. B. Large-scale oxidations in the pharmaceutical industry. *Chemical Reviews*, 106(7):2943-2989, 2006.

9. Toru, T. and Bolm, C. *Organosulfur Chemistry in Asymmetric Synthesis*. John Wiley & Sons, 2008.

10. Patai, S., Rappoport, Z., and Stirling, C. *The Chemistry of Sulfones, Sulfoxides and Cyclic Sulfides*. Wiley, Chichester, UK, 1994.

11. Legros, J., Dehli, J. R., and Bolm, C. Applications of catalytic asymmetric sulfide oxidations to the syntheses of biologically active sulfoxides. *Advanced Synthesis & Catalysis*, 347(1):19-31, 2005.

12. Collins, F. M., Lucy, A. R., and Sharp, C. Oxidative desulphurisation of oils via hydrogen peroxide and heteropolyanion catalysis. *Journal of Molecular Catalysis A: Chemical*, 117(1-3):397-403, 1997.

13. Maurya, M. R., Arya, A., Kumar, A., Kuznetsov, M. L., Avecilla, F., and Pessoa, J. C. Polymer-bound oxidovanadium(IV) and dioxidovanadium(V) complexes as catalysts for the oxidative desulfurization of model fuel diesel. *Inorganic Chemistry*, 49(14):6586-6600, 2010.

14. Tavakolian, M., Vahdati-Khajeh, S., and Asgari, S. Recent advances in solvent-free asymmetric catalysis. *ChemCatChem*, 11(13):2943-2977, 2019.

15. Heydari, N., Bikas, R., Shaterian, M., and Lis, T. Green solvent free epoxidation of olefins by a heterogenised hydrazone-dioxidotungsten(VI) coordination compound. *RSC Advances*, 12(8):4813-4827, 2022.

16. Paul, L., Banerjee, B., Bhaumik, A., and Ali, M. Solvent-free environmentally benign approach for the selective olefin epoxidation catalyzed by Mn(III)-immobilized mesoporous nanoarchitectonics. *Journal of Nanoscience and Nanotechnology*, 20(5):2858-2866, 2020.

17. Annese, C., Caputo, D., D'Accolti, L., Fusco, C., Nacci, A., Rossin, A., Tuci, G., and Giambastiani, G. Dioxomolybdenum(VI) complexes with salicylamide ligands: Synthesis, structure, and catalysis in the epoxidation of olefins under eco-friendly conditions. *European Journal of Inorganic Chemistry*, 2019(2):221-229, 2019.

18. Wang, Y., Gayet, F., Guillo, P., and Agustin, D. Organic solvent-free olefins and alcohols (ep) oxidation using recoverable catalysts based on $[PM_{12}O_{40}]^{3-}$ (M= Mo or W) ionically grafted on amino functionalized silica nanobeads. *Materials*, 12(20):3278, 2019.

19. Zare, M. and Moradi-Shoeili, Z. Oxidation of alkenes catalysed by molybdenum(VI)–oxodiperoxo complex anchored on the surface of magnetic nanoparticles under solvent-free conditions. *Applied Organometallic Chemistry*, 31(6):e3611, 2017.

20. Wang, W., Agustin, D., and Poli, R. Influence of ligand substitution on molybdenum catalysts with tridentate Schiff base ligands for the organic solvent-free oxidation of limonene using aqueous TBHP as oxidant. *Molecular Catalysis*, 443:52-59, 2017.

21. Paul, L., Banerjee, B., Bhaumik, A., and Ali, M. Functionalized SBA-15 supported nickel(II)–oxime–imine catalysts for liquid phase oxidation of olefins under solvent-free conditions. *Journal of Solid State Chemistry*, 237:105-112, 2016.

22. Shringarpure, P. A. and Patel, A. Supported undecaphosphotungstate: An ecofriendly and efficient solid catalyst for nonsolvent liquid-phase aerobic epoxidation of alkenes. *Industrial & Engineering Chemistry Research*, 50(15):9069-9076, 2011.

23. Nandi, M. and Talukdar, A. K. Vanadia loaded hierarchical ZSM-5 zeolite: A promising catalyst for epoxidation of cyclohexene under solvent free condition. *Journal of Porous Materials*, 23:1143-1154, 2016.

24. Gallo, J. M. R., Paulino, I. S., and Schuchardt, U. Cyclooctene epoxidation using Nb-MCM-41 and Ti-MCM-41 synthesized at room temperature. *Applied Catalysis A: General*, 266(2):223-227, 2004.

25. Thornburg, N. E., Thompson, A. B., and Notestein, J. M. Periodic trends in highly dispersed groups IV and V supported metal oxide catalysts for alkene epoxidation with H_2O_2. *ACS Catalysis*, 5(9):5077-5088, 2015.

26. Tiozzo, C., Bisio, C., Carniato, F., and Guidotti, M. Grafted non-ordered niobium-silica materials: Versatile catalysts for the selective epoxidation of various unsaturated fine chemicals. *Catalysis Today*, 235:49-57, 2014.

27. Ivanchikova, I. D., Skobelev, I. Y., Maksimchuk, N. V., Paukshtis, E. A., Shashkov, M. V., and Kholdeeva, O. A. Toward understanding the unusual reactivity of mesoporous niobium silicates in epoxidation of C=C bonds with hydrogen peroxide. *Journal of Catalysis*, 356:85-99, 2017.

28. Kang, S., Miao, R., Guo, J., and Fu, J. Sustainable production of fuels and chemicals from biomass over niobium based catalysts: A review. *Catalysis Today*, 374:61-76, 2021.

29. Ziolek, M. Niobium-containing catalysts—the state of the art. *Catalysis Today*, 78(1-4):47-64, 2003.

30. Selvaraj, M., Kawi, S., Park, D., and Ha, C. A merit synthesis of well-ordered two-dimensional mesoporous niobium silicate materials with enhanced hydrothermal stability and catalytic activity. *The Journal of Physical Chemistry C*, 113(18):7743-7749, 2009.

31. Thornburg, N. E., Nauert, S. L., Thompson, A. B., and Notestein, J. M. Synthesis−structure–function relationships of silica-supported niobium(V) catalysts for alkene epoxidation with H_2O_2. *ACS Catalysis*, 6(9):6124-6134, 2016.

32. Gallo, A., Tiozzo, C., Psaro, R., Carniato, F., and Guidotti, M. Niobium metallocenes deposited onto mesoporous silica via dry impregnation as catalysts for selective epoxidation of alkenes. *Journal of Catalysis*, 298:77-83, 2013.

33. Ivanchikova, I. D., Maksimchuk, N. V., Skobelev, I. Y., Kaichev, V. V., and Kholdeeva, O. A. Mesoporous niobium-silicates prepared by evaporation-induced

self-assembly as catalysts for selective oxidations with aqueous H_2O_2. *Journal of Catalysis*, 332:138-148, 2015.

34. Tiozzo, C., Bisio, C., Carniato, F., Gallo, A., Scott, S. L., Psaro, R., and Guidotti, M. Niobium–silica catalysts for the selective epoxidation of cyclic alkenes: The generation of the active site by grafting niobocene dichloride. *Physical Chemistry Chemical Physics*, 15(32):13354-13362, 2013.

35. Somma, F., Canton, P., and Strukul, G. Effect of the matrix in niobium-based aerogel catalysts for the selective oxidation of olefins with hydrogen peroxide. *Journal of Catalysis*, 229(2):490-498, 2005.

36. Aronne, A., Turco, M., Bagnasco, G., Ramis, G., Santacesaria, E., Di Serio, M., Marenna, E., Bevilacqua, M., Cammarano, C., and Fanelli, E. Gel derived niobium–silicon mixed oxides: Characterization and catalytic activity for cyclooctene epoxidation. *Applied Catalysis A: General*, 347(2):179-185, 2008.

37. Feliczak-Guzik, A. and Nowak, I. Mesoporous niobosilicates serving as catalysts for synthesis of fragrances. *Catalysis Today*, 142(3-4):288-292, 2009.

38. Gallo, J. M. R., Pastore, H. O., and Schuchardt, U. Study of the effect of the base, the silica and the niobium sources on the [Nb]-MCM-41 synthesized at room temperature. *Journal of Non-Crystalline Solids*, 354(15-16):1648-1653, 2008.

39. Lin, M.-L., Hara, K., Okubo, Y., Yanagi, M., Nambu, H., and Fukuoka, A. Remarkable effect of ordered mesoporous carbon support in tantalum oxide-catalyzed selective epoxidation of cyclooctene. *Catalysis Communications*, 12(13):1228-1230, 2011.

40. Nowak, I., Feliczak, A., Nekoksová, I., and Čejka, J. Comparison of oxidation properties of Nb and Sn in mesoporous molecular sieves. *Applied Catalysis A: General*, 321(1):40-48, 2007.

41. Popa, A., Ilia, G., Iliescu, S., Plesu, N., Ene, R., and Parvulescu, V. Styrene-co-divinylbenzene/silica hybrid supports for immobilization transitional metals and their application in catalysis. *Polymer Bulletin*, 76:139-152, 2019.

42. Nasrollahzadeh, M., Soleimani, F., Bidgoli, N. S. S., Nezafat, Z., Orooji, Y., and Baran, T. Recent developments in polymer-supported ruthenium nanoparticles/complexes for oxidation reactions. *Journal of Organometallic Chemistry*, 933:121658, 2021.

43. Maurya, M. R., Kumar, A., and Pessoa, J. C. Vanadium complexes immobilized on solid supports and their use as catalysts for oxidation and functionalization of alkanes and alkenes. *Coordination Chemistry Reviews*, 255(19-20):2315-2344, 2011.

44. Zhao, X., Bao, X. Y., Guo, W., and Lee, F. Y. Immobilizing catalysts on porous materials. *Materials Today*, 9(3):32-39, 2006.

45. Pessoa, J. C. and Maurya, M. R. Vanadium complexes supported on organic polymers as sustainable systems for catalytic oxidations. *Inorganica Chimica Acta*, 455:415-428, 2017.

46. Gupta, K. C., Sutar, A. K., and Lin, C.-C. Polymer-supported Schiff base complexes in oxidation reactions. *Coordination Chemistry Reviews*, 253(13-14):1926-1946, 2009.

47. Wang, B., Lin, J., Xia, C., and Sun, W. Porous organic polymer-supported manganese catalysts with tunable wettability for efficient oxidation of secondary alcohols. *Journal of Catalysis*, 406:87-95, 2022.

48. Boruah, J. J., Das, S. P., Ankireddy, S. R., Gogoi, S. R., and Islam, N. S. Merrifield resin supported peroxomolybdenum(VI) compounds: Recoverable heterogeneous catalysts for the efficient, selective and mild oxidation of organic sulfides with H_2O_2. *Green Chemistry*, 15(10):2944-2959, 2013.

49. Saikia, G., Ahmed, K., Rajkhowa, C., Sharma, M., Talukdar, H., and Islam, N. S. Polymer immobilized tantalum(v)–amino acid complexes as selective and recyclable heterogeneous catalysts for oxidation of olefins and sulfides with aqueous H_2O_2. *New Journal of Chemistry*, 43(44):17251-17266, 2019.

50. Evtushok, V. Y., Ivanchikova, I. D., Lopatkin, V. A., Maksimchuk, N. V., Podyacheva, O. Y., Suboch, A. N., Stonkus, O. A., and Kholdeeva, O. A. Heterolytic alkene oxidation with H_2O_2 catalyzed by Nb-substituted Lindqvist tungstates immobilized on carbon nanotubes. *Catalysis Science & Technology*, 11(9):3198-3207, 2021.

51. Thomas, J. M. *Design and Applications of Single-site Heterogeneous Catalysts: Contributions to Green Chemistry, Clean Technology and Sustainability*. World Scientific Publishing Company, 2012.

52. Valodkar, V. B., Tembe, G. L., Ravindranathan, M., Ram, R., and Rama, H. A study of synthesis, characterization and catalytic hydrogenation by polymer anchored

Pd(II)-amino acid complexes. *Journal of Molecular Catalysis A: Chemical*, 202(1-2):47-64, 2003.

53. Passoni, L. C., Siddiqui, M. R. H., Steiner, A., and Kozhevnikov, I. V. Niobium peroxo compounds as catalysts for liquid-phase oxidation with hydrogen peroxide. *Journal of Molecular Catalysis A: Chemical*, 153(1-2):103-108, 2000.

54. Bayot, D. and Devillers, M. Peroxo complexes of niobium(V) and tantalum(V). *Coordination Chemistry Reviews*, 250(19-20):2610-2626, 2006.

55. Gogoi, S. R., Boruah, J. J., Sengupta, G., Saikia, G., Ahmed, K., Bania, K. K., and Islam, N. S. Peroxoniobium(V)-catalyzed selective oxidation of sulfides with hydrogen peroxide in water: A sustainable approach. *Catalysis Science & Technology*, 5(1):595-610, 2015.

56. Li, S., Wang, K., Chang, K.-C. A., Zong, M., Wang, J., Cao, Y., Bai, Y., Wei, T., and Zhang, Z. Preparation and evaluation of nano-hydroxyapatite/poly (styrene-divinylbenzene) porous microsphere for aspirin carrier. *Science China Chemistry*, 55:1134-1139, 2012.

57. Kim, J.-W., Kim, K.-J., Park, S.-Y., Jeong, K.-U., and Lee, M.-H. Preparation and characterizations of C_{60}/polystyrene composite particle containing pristine C 60 clusters. *Bulletin of the Korean Chemical Society*, 33(9):2966-2970, 2012.

58. Atashbar, M., Sun, H., Gong, B., Wlodarski, W., and Lamb, R. XPS study of Nb-doped oxygen sensing TiO_2 thin films prepared by sol-gel method. *Thin Solid Films*, 326(1-2):238-244, 1998.

59. García-Sancho, C., Sádaba, I., Moreno-Tost, R., Mérida-Robles, J., Santamaría-González, J., López-Granados, M., and Maireles-Torres, P. Dehydration of xylose to furfural over MCM-41-supported niobium-oxide catalysts. *ChemSusChem*, 6(4):635-642, 2013.

60. Brunauer, S., Emmett, P. H., and Teller, E. Adsorption of gases in multimolecular layers. *Journal of the American Chemical Society*, 60(2):309-319, 1938.

61. Boruah, J. J. and Das, S. P. Solventless, selective and catalytic oxidation of primary, secondary and benzylic alcohols by a Merrifield resin supported molybdenum(vi) complex with H_2O_2 as an oxidant. *RSC Advances*, 8(60):34491-34504, 2018.

62. Li, Y., Fu, X., Gong, B., Zou, X., Tu, X., and Chen, J. Synthesis of novel immobilized tridentate Schiff base dioxomolybdenum(VI) complexes as efficient and reusable

catalysts for epoxidation of unfunctionalized olefins. *Journal of Molecular Catalysis A: Chemical*, 322(1-2):55-62, 2010.

63. Gong, B., Fu, X., Chen, J., Li, Y., Zou, X., Tu, X., Ding, P., and Ma, L. Synthesis of a new type of immobilized chiral salen Mn(III) complex as effective catalysts for asymmetric epoxidation of unfunctionalized olefins. *Journal of Catalysis*, 262(1):9-17, 2009.

64. Valodkar, V. B., Tembe, G. L., Ravindranathan, M., and Rama, H. Catalytic epoxidation of olefins by polymer-anchored amino acid ruthenium complexes. *Reactive and Functional Polymers*, 56(1):1-15, 2003.

65. Nakamoto, K. *Infrared and Raman Spectra of Inorganic and Co-ordination Compounds, Part B*. Wiley and Sons, New York, 1997.

66. Casado, J., López Navarrete, J., and Ramirez, F. Infrared and Raman spectra of L-asparagine and L-asparagine-d_5 in the solid state. *Journal of Raman Spectroscopy*, 26(11):1003-1008, 1995.

67. Masilamani, S., Ilayabarathi, P., Maadeswaran, P., Chandrasekaran, J., and Tamilarasan, K. Synthesis, growth and characterization of a novel semiorganic nonlinear optical single crystal: l-Asparagine cadmium chloride monohydrate. *Optik*, 123(14):1304-1306, 2012.

68. Venyaminov, S. Y. and Kalnin, N. Quantitative IR spectrophotometry of peptide compounds in water (H_2O) solutions. I. Spectral parameters of amino acid residue absorption bands. *Biopolymers: Original Research on Biomolecules*, 30(13-14):1243-1257, 1990.

69. Djordjevic, C. and Vuletic, N. Coordination complexes of niobium and tantalum. V. Eight-coordinated di-and triperoxoniobates(V) and-tantalates(V) with some nitrogen and oxygen bidentate ligands. *Inorganic Chemistry*, 7(9):1864-1868, 1968.

70. Bayot, D., Devillers, M., and Peeters, D. Vibrational spectra of eight-coordinate niobium and tantalum complexes with peroxo ligands: A theoretical simulation. *European Journal of Inorganic Chemistry*, 4118–4123, 2005.

71. Gao, L., Deng, K., Zheng, J., Liu, B., and Zhang, Z. Efficient oxidation of biomass derived 5-hydroxymethylfurfural into 2, 5-furandicarboxylic acid catalyzed by Merrifield resin supported cobalt porphyrin. *Chemical Engineering Journal*, 270:444-449, 2015.

72. Silverstein, R. M. and Bassler, G. C. Spectrometric identification of organic compounds. *Journal of Chemical Education*, 39(11):546, 1962.

73. Maniatakou, A., Makedonas, C., Mitsopoulou, C. A., Raptopoulou, C., Rizopoulou, I., Terzis, A., and Karaliota, A. Synthesis, structural and DFT studies of a peroxo-niobate complex of the biological ligand 2-quinaldic acid. *Polyhedron*, 27(16):3398-3408, 2008.

74. Narendar, Y. and Messing, G. L. Synthesis, decomposition and crystallization characteristics of peroxo-citrato-niobium: An aqueous niobium precursor. *Chemistry of Materials*, 9(2):580-587, 1997.

75. Lorgé, F., Wagner, A., and Mioskowski, C. Improved procedure for routine ^{13}C NMR analysis of Merrifield resin bound molecules. *Journal of Combinatorial Chemistry*, 1(1):25-27, 1999.

76. Mohanraj, S. and Ford, W. T. Analysis of cross-linking of poly [(chloromethyl) styrene] by high-resolution carbon-13 NMR spectroscopy. *Macromolecules*, 18(3):351-356, 1985.

77. LeTiran, A., Stables, J. P., and Kohn, H. Functionalized amino acid anticonvulsants: Synthesis and pharmacological evaluation of conformationally restricted analogues. *Bioorganic & Medicinal Chemistry*, 9(10):2693-2708, 2001.

78. Jacobson, S. E., Tang, R., and Mares, F. Group 6 transition metal peroxo complexes stabilized by polydentate pyridinecarboxylate ligands. *Inorganic Chemistry*, 17(11):3055-3063, 1978.

79. Pettersson, L., Andersson, I., and Gorzsás, A. Speciation in peroxovanadate systems. *Coordination Chemistry Reviews*, 237(1-2):77-87, 2003.

80. Rodante, F., Marrosu, G., and Catalani, G. Thermal analysis of some α-amino acids with similar structures. *Thermochimica Acta*, 194:197-213, 1992.

81. Weiss, I. M., Muth, C., Drumm, R., and Kirchner, H. O. Thermal decomposition of the amino acids glycine, cysteine, aspartic acid, asparagine, glutamic acid, glutamine, arginine and histidine. *BMC Biophysics*, 11(1):1-15, 2018.

82. Mukherjee, A. and Biswas, M. Thermal characteristics of iron(III), cobalt(II), and copper(II) complexes of dipyridylamine anchored on polystyrene-divinylbenzene copolymer. *Journal of Applied Polymer Science*, 50(9):1485-1492, 1993.

83. Lomozik, L. and Wojciechowska, A. Comparative studies of the coordination mode in complexes of copper with asparagine and copper with aspartic acid in solution and solid state. *Polyhedron*, 8(1):1-6, 1989.

84. Lim, M. C. Mixed-ligand complexes of palladium(II). Part 2. Diaqua (ethylenediamine) palladium(II) complexes of L-asparagine and L-glutamine. *Journal of the Chemical Society, Dalton Transactions*, (14):1398-1400, 1977.

85. Sovago, I., Kallay, C., and Varnagy, K. Peptides as complexing agents: Factors influencing the structure and thermodynamic stability of peptide complexes. *Coordination Chemistry Reviews*, 256(19-20):2225-2233, 2012.

86. Dengel, A. C. and Griffith, W. P. Studies on Transition metal peroxo complexes—IX. Carboxylato peroxo complexes of niobium(V), tantalum(V), zirconium(IV) and hafnium(IV). *Polyhedron*, 8(11):1371-1377, 1989.

87. Ramanathan, A., Maheswari, R., and Subramaniam, B. Facile styrene epoxidation with H_2O_2 over novel niobium containing cage type mesoporous silicate, Nb-KIT-5. *Topics in Catalysis*, 58:314-324, 2015.

88. Lin, C. C., Smith, F. R., Ichikawa, N., Baba, T., and Itow, M. Decomposition of hydrogen peroxide in aqueous solutions at elevated temperatures. *International Journal of Chemical Kinetics*, 23(11):971-987, 1991.

89. Gogoi, S. R., Ahmed, K., Saikia, G., and Islam, N. S. Macromolecular metal complexes of Nb^V as recoverable catalysts for selective and eco-compatible oxidation of organic sulfides in water. *Journal of Indian Chemical Society*, 95:801-812, 2018.

90. Arizaga, B., de Leon, A., Burgueno, N., Lopez, A., Paz, D., Martínez, N., Lorenzo, D., Dellacassa, E., and Bussi, J. A clean process for the production of oxygenated limonene derivatives starting from orange oil. *Journal of Chemical Technology & Biotechnology*, 82(6):532-538, 2007.

91. Carniti, P., Gervasini, A., Tiozzo, C., and Guidotti, M. Niobium-containing hydroxyapatites as amphoteric catalysts: Synthesis, properties, and activity. *ACS Catalysis*, 4(2):469-479, 2014.

92. Bonchio, M., Conte, V., Assunta de Conciliis, M. A., Di Furia, F., Ballistreri, F. P., Tomaselli, G. A., and Toscano, R. M. The relative reactivity of thioethers and sulfoxides toward oxygen transfer reagents: The oxidation of thianthrene 5-oxide and related compounds by MoO_5HMPT. *The Journal of Organic Chemistry*, 60(14):4475-4480, 1995.

93. Conte, V. and Bortolini, O. The Chemistry of Peroxides – Transition Metal Peroxides. Synthesis and Role in Oxidation Reactions, Wiley Interscience, 2006.

94. Cordeiro, P. J. and Tilley, T. D. Enhancement of epoxidation efficiencies for Ta-SBA15 catalysts. The influence of modification with–EMe_3 (E= Si, Ge, Sn) groups. *Langmuir*, 27(10):6295-6304, 2011.

95. Salem, I. A., El-Maazawi, M., and Zaki, A. B. Kinetics and mechanisms of decomposition reaction of hydrogen peroxide in presence of metal complexes. *International Journal of Chemical Kinetics*, 32(11):643-666, 2000.

96. Hulea, V., Maciuca, A.-L., Fajula, F., and Dumitriu, E. Catalytic oxidation of thiophenes and thioethers with hydrogen peroxide in the presence of W-containing layered double hydroxides. *Applied Catalysis A: General*, 313(2):200-207, 2006.

97. Sherrington, D. C. Polymer-supported metal complex alkene epoxidation catalysts. *Catalysis Today*, 57(1-2):87-104, 2000.

98. Sharpless, K., Townsend, J., and Williams, D. Mechanism of epoxidation of olefins by covalent peroxides of molybdenum(VI). *Journal of the American Chemical Society*, 94(1):295-296, 1972.

99. Yudanov, I. Mechanism of olefin epoxidation with transition metal peroxo complexes: DFT study. *Journal of Structural Chemistry*, 48:S111-S124, 2007.

100. Gisdakis, P., Yudanov, I. V., and Rösch, N. Olefin epoxidation by molybdenum and rhenium peroxo and hydroperoxo compounds: A density functional study of energetics and mechanisms. *Inorganic Chemistry*, 40(15):3755-3765, 2001.

101. Amini, M., Haghdoost, M. M., and Bagherzadeh, M. Oxido-peroxido molybdenum(VI) complexes in catalytic and stoichiometric oxidations. *Coordination Chemistry Reviews*, 257(7-8):1093-1121, 2013.

102. Ma, W., Yuan, H., Wang, H., Zhou, Q., Kong, K., Li, D., Yao, Y., and Hou, Z. Identifying catalytically active mononuclear peroxoniobate anion of ionic liquids in the epoxidation of olefins. *ACS Catalysis*, 8(5):4645-4659, 2018.

103. Ding, B., Zhang, R., Zhou, Q., Ma, W., Zheng, A., Li, D., Yao, Y., and Hou, Z. Olefin epoxidation with ionic liquid catalysts formed by supramolecular interactions. *Molecular Catalysis*, 500:111342, 2021.

104. Kholdeeva, O. A., Ivanchikova, I. D., Maksimchuk, N. V., and Skobelev, I. Y. H_2O_2-based selective epoxidations: Nb-silicates versus Ti-silicates. *Catalysis Today*, 333:63-70, 2019.

105. Maksimchuk, N. V., Maksimov, G. M., Evtushok, V. Y., Ivanchikova, I. D., Chesalov, Y. A., Maksimovskaya, R. I., Kholdeeva, O. A., Sole-Daura, A., Poblet, J. M., and Carbo, J. J. Relevance of protons in heterolytic activation of H_2O_2 over Nb(V): Insights from model studies on Nb-substituted polyoxometalates. *ACS Catalysis*, 8(10):9722-9737, 2018.

106. Chagas, P., Oliveira, H. S., Mambrini, R., Le Hyaric, M., de Almeida, M. V., and Oliveira, L. C. A novel hydrofobic niobium oxyhydroxide as catalyst: Selective cyclohexene oxidation to epoxide. *Applied Catalysis A: General*, 454:88-92, 2013.

107. Shima, H., Tanaka, M., Imai, H., Yokoi, T., Tatsumi, T., and Kondo, J. N. IR observation of selective oxidation of cyclohexene with H_2O_2 over mesoporous Nb_2O_5. *The Journal of Physical Chemistry C*, 113(52):21693-21699, 2009.

108. Sato, K., Hyodo, M., Aoki, M., Zheng, X.-Q., and Noyori, R. Oxidation of sulfides to sulfoxides and sulfones with 30% hydrogen peroxide under organic solvent-and halogen-free conditions. *Tetrahedron*, 57(13), 2469-2476, 2001.

109. Choudary, B., Bharathi, B., Reddy, C. V., and Kantam, M. L. Tungstate-exchanged Mg-Al-LDH catalyst: An eco-compatible route for the oxidation of sulfides in aqueous medium. *Journal of the Chemical Society, Perkin Transactions 1*, (18):2069-2074, 2002.

110. Maniatakou, A., Karaliota, S., Mavri, M., Raptopoulou, C., Terzis, A., and Karaliota, A. Synthesis, characterization and crystal structure of novel mononuclear peroxotungsten(VI) complexes. Insulinomimetic activity of W(VI) and Nb(V) peroxo complexes. *Journal of Inorganic Biochemistry*, 103(5):859-868, 2009.